Predicting thumb osteoarthrosis using morphology: a 3D statistical shape analysis

Ana Bandarrinha Brandão

Thesis to obtain the Master of Science Degree in

Biomedical Engineering

Supervisors: Prof. Carlos Miguel Fernandes Quental

Dr. Angela Kedgley

Examination Committee

Chairperson: Prof. Fernando Manuel Fernandes Simões

Supervisor: Prof. Carlos Miguel Fernandes Quental

Member of the Committee: Prof. João Orlando Marques Gameiro Folgado

October 2019

Preface

The work presented in this thesis was performed at the Upper Limb Biomechanics research group laboratory at Imperial College London (London, UK), during the period February 2019-July 2019, under the supervision of Dr. Angela Kedgley, Senior Lecturer, and Wan Rusli, PhD Candidate, and within the frame of the Erasmus Placement. The thesis was co-supervised at Instituto Superior Técnico by Prof. Carlos Miguel Fernandes Quental.

Declaration

I declare that this document is an original work of my own authorship and that it fulfils all the requirements of the Code of Conduct and Good Practices of the Universidade de Lisboa.

Acknowledgments

First, I would like to thank Dr. Angela Kedgley, for giving me the opportunity of making my master thesis abroad, in Imperial College London. Working along with her research group, where I was so well received and integrated was a great experience that I cherish. I would also thank Wan Rusli for the guidance he provided and his patient explanations. Thanks also to Prof Crisco's research group at Brown University that provided the dataset that made this research possible.

I would like to thank Prof. Carlos Quental for being available from day one. For being so supportive, helpful and collaborative throughout this process. Despite not being his main field of research, he supervised me as it was.

I would like to thank my parents, Conceição and Vitor, who taught me strength and resilience to overcome all obstacles, to be focused and to thrive. They provide for everything, allowing me to pursue my goals, supporting me in every decision and being my number one cheerleaders. To my mum I thank for the sweet words she always offers me. To my dad I thank for always pushing for me. Together they form the perfect equilibrium, that I will always need.

To my brothers and sister, Nuno, Miguel and Inês, thank you for shaping the person I am. I would not change a thing in having you as my siblings. To Nuno, my home and rock in London, thank you for your protection and honesty. To Miguel, who always has something to teach, thank you for your companionship. To Inês, who always has a warm hug ready, thank you for your love.

To Luís, thank you for making easy what not always is. You have always listened to every little thing comforted and believed in me. During this journey, you have been my biggest ally in every challenge, this would not be possible without you.

My dearest friends, the family that I have chosen. To the friends I kept since middle school, that are part of me and know me like no one does, thank you for being always there. The friends I met through volunteering, that turned my world upside down, thank you for cheering me up. And the friends with whom I shared university. This is our final step, thank you for walking along with me, this is both mine and yours.

Resumo

O desenvolvimento da osteoartrite está relacionado com variações morfológicas em várias articulações, no entanto, esta correlação ainda não está provada na osteoartrite do polegar. Propôs-se no presente trabalho encontrar variações morfológicas na primeira articulação carpometacarpal, composta pelo primeiro metacarpo e trapézio, que possam estar relacionadas com o desenvolvimento de osteoartrite. Para o efeito usou-se statistical shape modelling para analisar a variação na forma desta articulação em três populações duas das quais com patologias. A primeira com patologia progressiva, onde o nível de osteoartrite subiu de I para II no período em análise, e a segunda com a patologia estabilizada, onde a osteoartrite se manteve no estado I durante aquele período. O terceiro grupo, de controle, é constituído por indivíduos saudáveis.

Utilizou-se uma abordagem qualitativa e quantitativa para analisar as diferenças entre populações. A abordagem qualitativa teve como objetivo a comparação de dois modelos, baseada na distância que os separa e assinalando os locais onde existem diferenças. A abordagem quantitativa resultou da medição de quatro parâmetros morfológicos, nomeadamente os ângulos inclinação e torsão do primeiro metacarpo e a largura e altura da face articular do trapézio.

A população com patologia tende a ter o primeiro metacarpo mais curto e mais espesso e a superfície da articulação do trapézio mais convexa. Acerca dos parâmetros morfológicos medidos, no ângulo inclinação encontraram-se diferenças significativas entre a população saudável e a patológica, o que suporta a hipótese de que a forma deste osso pode ajudar a prever osteoartrite.

Palavras-chave: primeira articulação carpometacarpo, osteoartrite em estado inicial, statistical shape modeling, preditor de osteoartrite, angulo de inclinação, morfologia

Abstract

Shape variations are linked with the development of osteoarthritis in various joints, but the correlation between morphologic variations and osteoarthritis in the thumb, is not yet proven. The purpose of the present work was to find morphologic variations in the first carpometacarpal joint, composed of the first metacarpal and trapezium, that could be correlated with the development of osteoarthritis. This was achieved by using multi-object statistical shape modelling to analyse the variation in shape within, and between, three populations, including two pathological populations: a progressive one, where the osteoarthritis level increased from I to II over time; and a stabilised population where the osteoarthritis remained in stage I through time. The control group consisted in a healthy population that did not develop osteoarthritis over time.

The analysis of the differences amongst populations was conducted by a qualitative and quantitative approach. The qualitative approach aimed to compare two bone models based on a distance map that point out the sites where there were differences. The quantitative approach resulted in the measurement of four morphologic parameters, namely the tilt angle, torsion angle on the first metacarpal and width and length on the trapezium.

Despite the variability in bone shape, pathological people tended to have the first metacarpal shorter and thicker and the articulating surface of the trapezium more convex. Regarding the morphological parameters, the tilt angle was found to be significantly different between healthy and stabilised populations, which supports the hypothesis that bone shape may help predict osteoarthritis.

Key words: First carpometacarpal joint, early stage osteoarthrosis, statistical shape modelling, osteoarthrosis predictor, tilt angle, morphology

TABLE OF CONTENTS

TABLE OF FIGURES

LIST OF TABLES

LIST OF ACRONYMS

AOL	Anterior Oblique Ligament
BMI	Body mass index
CMC	Carpometacarpal
CT	Computed Tomography
CPD	Coherent Point Drift
DRL	Dorsalradial Ligament
GMM	Gaussian Mixture Model
IML	Intermetacarpal Ligament
MRI	Magnetic Resonance imaging
OA	Osteoarthrosis
PC	Principal Component
PCA	Principal Component Analysis
PP	Projection Pursuit
PDM	Point model distribution
POL	Posterior Oblique Ligament
SD	Standard deviation
T0	Initial time
T1	Final time
UCL	Ulnar Collateral Ligament

1. INTRODUCTION

Osteoarthrosis (OA) is the most common joint disease in the world. Approximately 1.5 million people in the UK alone have sought treatment for OA of the hand or wrist, over a seven year period (Arthritis Research UK, 2013). Although this is not the most common site for OA, it is highly impairing in the late stages of disease (Kalichman, Hernández-Molina, 2010). The joint that most impairs hand function when affected by OA is the first carpometacarpal (CMC) joint, which is located at the base of the thumb. Being responsible for thumb mobility, it is fundamental for hand functionality. First CMC-OA diagnosis is a complex multifactorial process. It requires qualitative assessment of a patient's history of pain, physical assessment and a classifier. There are two classifiers: the Eaton that recognizes four stages of this condition through radiography of the thumb(Eaton *et al.*, 1984), and the Badia score that categorizes patients into three stages through an arthroscopy (Gillis, Calder & Williams, 2011). Despite the continual development and improvement of these tools, the diagnosis can be ambiguous, especially in the early stages of this condition (Neumann & Bielefeld, 2003).

Early detection of first CMC-OA is fundamental since this disease is only perceived when it is already having an impact on people's lives. Moreover, as this condition progresses, the impact on people's lives increases substantially. Developing methods that allow an early detection may have a great impact in delaying the evolution of the disease. The impact of this condition on daily routine is significant. Note that little hand movements like grasping, the most common daily hand movement performed (Schieber & Santello, 2004), becomes impossible to perform when this disease progresses.

Although first CMC-OA physiological, etiological and pathological mechanisms are not yet fully understood, there is research that supports the hypothesis that, amongst other factors, the shape of the bones in first CMC joint can be correlated with the development of OA (Schneider *et al.*, 2018). Yet, research is needed in order to reinforce this correlation, such as, quantitative parameters, that allow a more objective analysis. Often, the study of shape is performed, using statistical shape modelling (SSM). This method allows us to perceive the shape of a certain set of structures, giving as output, the mean model shape of this set of structures and its variations.

1.1 Motivation and objectives

The motivation behind this work was to find a predictor to identify early stage OA, based on the differences that might exist in bone shape. The identification of morphological predictors would allow prevention, stopping disease progression and/or increasing the treatment options based on the first CMC bone's shape.

This investigation was conducted through the application of a 3D multi-object SSM analysis on healthy and pathological populations. The objectives were to carry out quantitative and qualitative analyses in each population, followed by a comparative analysis to assess the differences in bone shape, in both approaches. The qualitative analysis was conducted by assessing the difference between two bone models. To perform the quantitative analysis, four morphologic parameters were measured. In the first metacarpal, the tilt and torsion angles and, in the trapezium articulating surface, the width and length were measured. Afterwards, the measured parameters were compared between healthy and pathological people. In order to verify if there was a parameter that correlates with OA development and/or evolution.

1.2 Thesis outline

The present document is divided into six chapters. Chapter 1 is the introduction, which gives the context and relevance to this work. The second chapter explains the theoretical concepts needed to understand the work developed. Moreover, it allows the reader to understand the ongoing state of the art on OA, highlighting the latest developments on the topic and showing the contributions of this work. The third chapter is related to the methodology followed, particularly the methods used to achieve the results and how they were analysed. In Chapter 4, the results of this study are presented. This chapter comprises qualitative and quantitative analyses. The first was based on a variety of qualitative comparisons between models, whereas the second was based on the measurement of specific morphological parameters of the two bones that form the joint. The fifth chapter is where the discussion of the results is made. The sixth chapter gathers the main conclusions. This chapter is essential since it states the novel contributions of this work and identifies future working directions. Apart from the described chapters, this document includes an appendix in which some additional and complementary results are depicted.

2. THEORETICAL BACKGROUND

In this chapter, the theoretical background concerning first CMC-OA characterization, diagnostic tools and research regarding the relation between bone morphology and OA development are exposed. Besides that, statistical shape analysis, the main method used in this work, is explained. The present chapter is essential in order to understand the chapters that follow, and especially to recognize the value and importance of the results obtained in this research.

2.1 First Carpometacarpal Joint

The most common musculoskeletal condition affecting older people is OA (Arthritis Research UK, 2013) and it is highly prevalent in the first CMC joint, which is the object of study of this work. To better comprehend its importance and its range of movements, it is necessary to have a basic understanding of its anatomy. In the next subsections the anatomy of the first CMC and OA are going to be explained, with emphasis on the effects of OA in the first CMC.

2.1.1 Anatomy

The first CMC joint, depicted in Figure 1, connects the base of the thumb to the wrist, and more precisely it joins the first metacarpal to the trapezium.

The first metacarpal is a long bone, it is smaller than the other metacarpal bones. This bone contains three main parts: the head that presents two condyles on the ulnar and radial regions and two protuberances on the dorsal region; the body or shaft; and the base, the articulating joint surface that presents a concave-convex surface for articulation with the trapezium. Although it has no facets on its sides, there is a tubercle for the insertion of the abductor pollicis longus muscle on its radial side (Gray & Lewis, 1918).

The trapezium is distinguished by a deep groove on its volar surface, located on the radial side of the carpus, between the scaphoid and the first metacarpal. The face under study, the one in contact with the first metacarpal, is the inferior surface, following the orthostatic position. This surface is oval, concave from side to side, convex from anterior to posterior, so as to form a saddle-shaped surface for articulation with the base of the first metacarpal (Gray & Lewis, 1918).

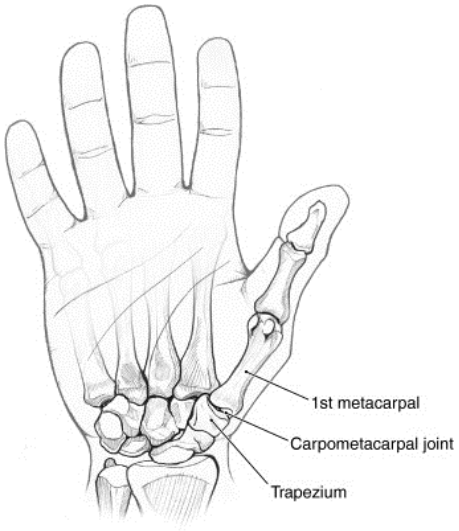

Figure 1- Hand bones highlighting carpometacarpal join composed of the first metacarpal and the trapezium (Waldman, 2009)

A joint is the structure in the human body at which two parts of the skeleton are fit together, allowing different types and degrees of movements. Depending on its function, joints can be qualified structurally, according to the type of binding tissue, and functionally, depending on the type and degree of movement allowed (Brand & Hollister, 1993).

There are four types of structural joints such as fibrous joints (a dense tissue rich in collagen fibres), cartilaginous joints (when bonded by cartilage), facet joints (in vertebrae) and finally, synovial joint (the bones are united by an irregular connective tissue, and this structure is ensured by accessory ligaments). The first CMC joint is a synovial joint (Tortora & Derrickson, 2014). Functionally, joints can be classified into three categories. From the stiffest to the freely mobile joint, there are synarthrosis, amphiarthrosis and diarthrosis or synovial joints. This last category, depicted in Figure 2 , contains six groups, according to the type of movement allowed (Betts *et al.*, 2013).

Unlike the second to the fifth CMC joints, that are classified as condyle joints (as in Figure 2 (d)) allowing flexion and extension. The first CMC joint is classified as saddle-shape joint (as in Figure 2 (f)), enabling flexion-extension and abduction-adduction. Combining these movements the thumb is capable of several other movements, such as, close lateral pinch, opposition, retropulsion, circumduction and prehension of large objects within the palm (Ladd *et al.*, 2013b; Melville *et al.*, 2015). The rotation and translation of this joint enables the pronation-supination movement. The first CMC joint maintains an equilibrium between stability and mobility: its mobility is allowed by a joint shape that lacks osseous constraint. On the other hand, stability is guaranteed by a ligamentous complex which is fundamental to the joint function. The joint is lax and incongruent in the resting position and stable and tightly congruent during full opposition (Ladd *et al.*, 2013b; Melville *et al.*, 2015).

Although sixteen different ligaments can be identified in the trapezium and first CMC joint, only five have been recognised as directly implicated in joint stability. These form the ligamentous complex: the anterior oblique ligament (AOL), the posterior oblique ligament (POL), the dorsoradial ligament (DRL),

the intermetacarpal ligament (IML) and the ulnar collateral ligament (UCL) (Cardoso *et al.*, 2009; Ladd *et al.*, 2013b; Lara, *et al.*, 2000); three of these are illustrated in Figure 3.

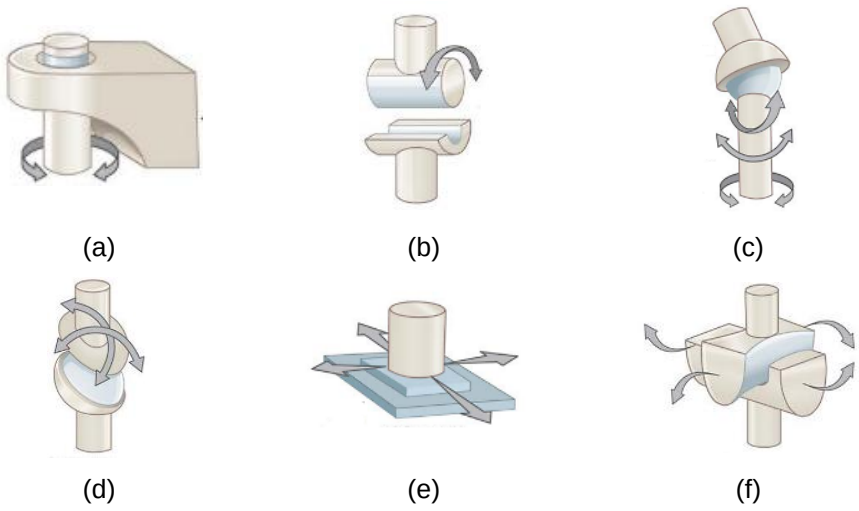

Figure 2 – Six types of synovial joints: (a) Pivot joint allows rotation around an axis. (b) Hinge joint is uniaxial, allowing bending and straightening. (c) Ball and socket joint is multiaxial. (d) Condyloid joint is biaxial and allows for two planes of movement. (e) Plane joint is multiaxial, though constrained (f) Saddle joint is biaxial. Adapted (Betts *et al.*, 2013)

Being that the DRL the strongest, widest and thickest ligament, it restrains the dorsal dislocation. It originates on the dorsal trapezium and inserts on the radial base of the thumb metacarpal. The AOL has a specific role in the stabilization of the thumb, since it is the resisting opposing force to abduction, extension and pronation. It originates on the distal trapezial tubercle and inserts on the ulnar base of the thumb metacarpal.

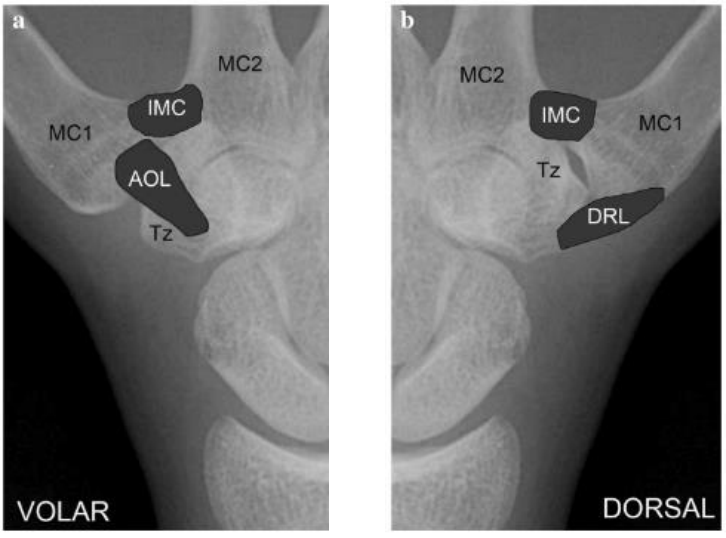

(a) (b)

Figure 3 - Thumb basal joint ligaments: (a) Volar view showing the anterior oblique ligament (AOL) and the intermetacarpal ligament (IMC), and (b) dorsal view showing the dorsoradial ligament (DRL) and the IMC again. (Melville *et al.*, 2015)

The IMC is extracapsular, it arises from the dorsoradial aspect of the second metacarpal and runs towards the volar-ulnar until insertion into the first metacarpal base. The POL is a capsular ligament that originates on the dorsal side of the trapezium and inserts in the dorsal and ulnar aspect of the first metacarpal, along with the IMC. Finally, the UCL, an extracapsular ligament, originates from the distal and ulnar margin of the flexor retinaculum insertion onto the trapezial ridge (Melville *et al.*, 2015; Cardoso *et al.*, 2009; Ladd *et al.*, 2013b).

Biomechanical studies have shown that joint reaction forces increase exponentially from the tip of the thumb to the CMC joint with grasp and forceful pinch. The joint reaction force at the base of the thumb is 12 times greater than that generated at the tip of the thumb with lateral pinch, and compressive forces can reach 120 kg and may occur at the CMC joint with forceful grasp (Ladd *et al.*, 2013a). In fact, smaller joints experience higher stresses because smaller bones have smaller contact areas, but activities of daily living require similar loads. Opening a jar, for example, demands a fixed torque, regardless of joint size. Bone size also affects the size of the muscle moment arms crossing the joint, a joint with lower aspect ratio (length to width) would require a larger force to generate the same torque due to a smaller moment arm, when compared to a joint with higher aspect ratio (Schneider *et al.*, 2018).

2.1.2 Osteoarthrosis

The most common joint disease is OA, affecting mostly middle aged and older people. It is characterized by joint pain, dysfunction and a decrease in the freedom of active joint movement (Hunter, Bierma-Zeinstra, 2006). In the latest stages, it also occurs due to joint contractures, muscle atrophies and limb deformation. This disease is characterized by a progressive loss of articular cartilage and degradation of the joint. This process involves the joint's inflammation and the body's attempt to repair it, which ultimately worsens the inflammation process leading to remodelling and sclerosis of subchondral bone and osteophyte formation (Hernández-Díaz, et al., 2017). As illustrated in Figure 4, the cartilage roughens and becomes thinner, the underlying bone thickens and grows, forming spurs, and the gap between bones becomes narrower. This, together with the excess of fluid in the joint capsule, causes the joint to swell, leading to the contraction of the ligaments around the joint (Arthritis Research UK, 2013).

Osteoarthrosis can be primary, or idiopathic, and, less frequently, secondary as a result of an injury or other disorder (Gray & Lewis, 1918). In the first condition, the most common, the causes of OA remain poorly understood. Nonetheless, there is set of risk factors that have been identified, such as age, gender, genetic factors, joint injury or disease, amongst others (Arthritis Research UK, 2013). From these, age and gender have been shown to be strongly related with the development of the disease (Cho et al., 2011; Riancho et al., 2010). More than a third of people over 45 years reports joint symptoms. These vary from a sensation of occasional joint stiffness and intermittent aching associated with activity, to permanent loss of motion and constant deep pain. However, for people over 65 years this percentage increases up to 75% (Hunter & Bierma-Zeinstra, 2006). This age relation could be explained by the loss of function of the chondrocytes, which are the cells responsible for maintaining and restoring the articular cartilage (Halilaj et al., 2015b). Women are six times more likely to develop OA when compared to men (Arthritis Research UK, 2013) and this difference could reside and be linked

to the biological differences between them, mainly in the reproductive hormones. The body weight is also a factor that influences the likelihood of developing arthrosis, mostly in joints that bare the body's weight, but even non-weight-bearing joints are negatively affected by a high body mass index (Weiss & Jurmain, 2007).

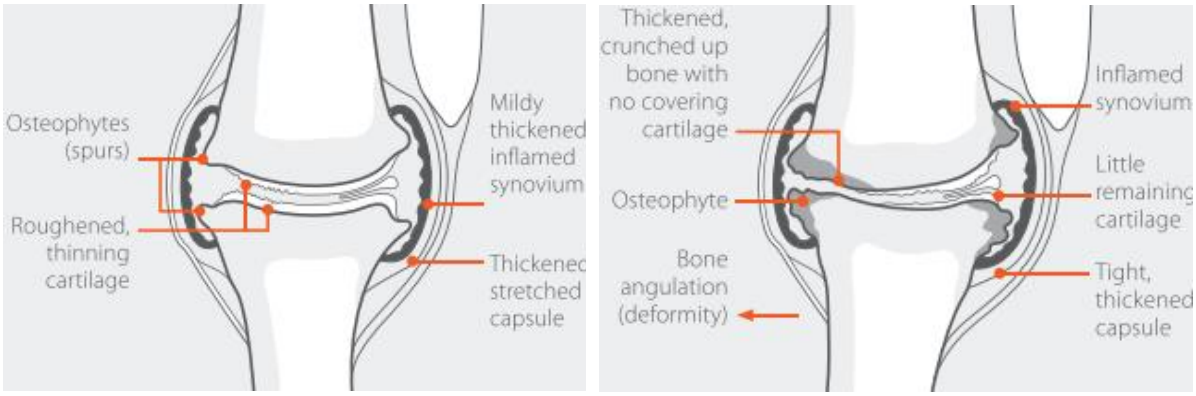

(a) (b)

Figure 4 - Process of osteoarthrosis progression. (a) a joint exhibiting mild OA. (b) joint that was deformed by severe OA (Arthritis Research UK, 2013)

As described in Section 2.1.1., the first CMC joint enables the thumb to have a diverse range of movements and, consequently, grants the hand movements that are essential to our daily routine. When the first CMC joint is affected by OA, the ability to perform tasks of everyday life may become impaired or lost altogether. Loss of thumb function imparts a 40% to 50% rate of impairment to the upper extremity because of its central role in nearly all grasping and handling manoeuvres (Ladd *et al.*, 2013a). In the first CMC joint, OA development is strongly linked with a genetic factor, although heavy manual work can also contribute for its development.

There are two theories of CMC-OA etiology: the ligamentous laxity and the joint impingement. The first states that with adjacent palmar degeneration of the trapezium, the AOL becomes lax, resulting in abnormal shear stress and degradation of the joint. The joint impingement theory affirms that the cause of OA is degeneration secondary to joint impingement during functional pinch and high contact stresses through pinch initiate or exacerbate OA (Kovler *et al.*, 2004). However, since there is no consensus in the literature, CMC-OA is characterized as a multifactorial disease, meaning that both theories can be correct simultaneously. It is even possible that other factors, not identified yet, can contribute to the development of CMC-OA.

2.2 Diagnosis of OA in the first CMC joint

This subsection intends to give understanding about the currently available tools to diagnose first CMC-OA. This allows to perceive the need for new diagnostic tools and to understand the patient's diagnosis involved in this thesis.

The clinical evaluation of CMC-OA does not rely on one single technique. It gathers the use of X-ray, or an arthroscopy, patient history of pain and dysfunction, and physical assessment. The diagnosis obtained is essential to guide the physician on treatment choices, since the course of the treatment is completely different depending on the OA stage.

When evaluating patient history of pain and dysfunction, it is essential to focus on the location, duration, onset, frequency, intensity and quality. Patients diagnosed with CMC-OA usually complain about symptom exacerbation with gripping and pinching activities. Understanding hand dominance and occupation is also important to frame the pain impact in the patient's life (Patel, Beredjiklian & Matzon, 2013).

There are a range of physical examinations that can be performed to assess hand functionality, such as the grind test, metacarpal flexion, metacarpal extension and pressure-shear tests for CMC-OA, in which the physician wants to know if the patients feel pain during the manoeuvres.

Arthroscopy is a minimally invasive technique where an arthroscope is inserted through a small incision near the joint (Menon, 1996). It allows evaluation of first CMC-OA and treatment in some cases. On one hand, this diagnostic tool is not only reliable but also allows the easy visualization of the joint. On the other hand, not all people can be eligible to undergo this procedure, and it requires greater time and resource consumption (Badia & Khanchandani, 2007).

The X-ray, the most used diagnostic tool, which allows the quantitative classification of CMC-OA according to the Eaton classification (Kubik & Lubahn, 2002; Eaton *et al.*, 1984). To apply the Eaton classifier, a lateral radiograph of the CMC joint of the thumb with the sesamoid bones superimposed on one another must be obtained first. Afterwards, a hand surgeon must analyse the radiography and categorize it in one of the four stages proposed by Eaton, which are illustrated in Figure 5.

These stages were created based on the shape, morphology and display of the first CMC joint using radiography. A radiograph is classified as stage I arthrosis, Figure 5A, when there is no joint space narrowing, cyst formation or subchondral changes. However, this stage might have joint space widening attributable to synovitis, effusion or laxity of the first CMC joint. Stage II OA, Figure 5B, is distinguished from stage I by featuring joint space narrowing with osteophytes or loose bodies smaller than 2 mm in diameter. This stage is often observed in active middle age women. Evidence of subluxation is already present. In stage III OA, Figure 5C, the subluxation is more prominent, and osteophytes exceed 2 mm in diameter. Besides, the joint space is even narrower and there is sclerotic bone and cystic changes. Stage IV OA, Figure 5D, the most severe one, exhibits advanced degenerative changes, such as substantial subluxation and joint narrowing. This stage is mainly characterized by the degradation of the scaphotrapezial joint, in addition to the already degraded CMC joint. (Kennedy, Manske & Huang, 2016).

Although the Eaton classification is the most used method, it has some limitations. Firstly, it is difficult to profile the thumb CMC joint radiographically since the thumb's orientation and trapezium shape make the assessment of OA more difficult in the coronal and sagittal planes. This can lead to over or underdiagnosing of OA, when compared with anatomic inspection and even with patient's pain levels (Kennedy, Manske & Huang, 2016). Secondly, other researchers (Dela Rosa, Vance, Stern, 2004) have suggested different hand positions during radiography or even more than one radiography to better

visualize the trapezium and obtain a more accurate diagnostic. Nonetheless, and despite not being quantitatively objective, Eaton classification is considered to be moderately reliable (Kubik, Lubahn, 2002).

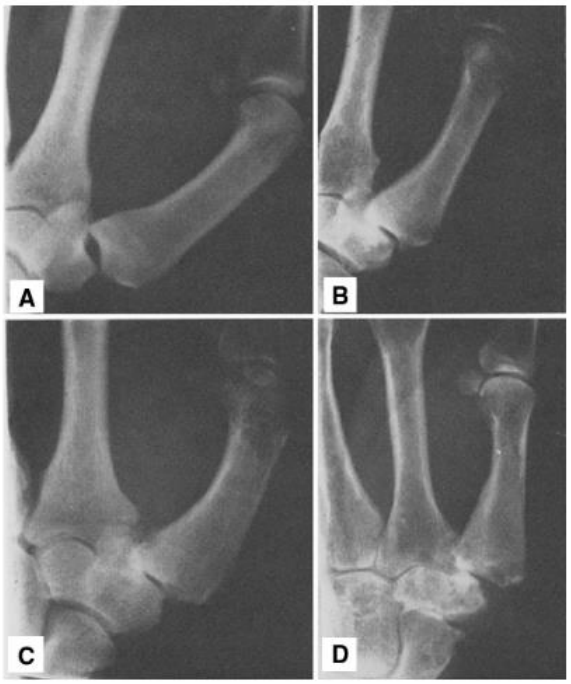

Figure 5 – Radiography of left hand in four subjects. Subject A stage I CMC-OA, subject B stage II CMC-OA, subject C stage III CMC-OA, subject D stage IV CMC-OA (Eaton *et al.*, 1984)

Finally, there are other forms of scanning the first CMC joint including 3D methods, like CT (Computed Tomography) scan or MRI (Magnetic Resonance Imaging), or even ultrasound. These techniques are used to overcome some of the limitations of the 2D analyses based on planar X-rays, making the analysis of joint degradation easier since there are no overlapping structures. Ultrasound and MRI have also been shown to be useful to detect ligamentous degradation (Li et al., 2016). Despite providing superior results, these 3D techniques continue to be used only in particular cases due to their drawbacks (Li *et al.*, 2016):

1. Ultrasound technology is a low-cost modality, and is particularly useful for the evaluation of synovitis; however, it lacks specificity and the ability to monitor soft tissue conditions;
2. MRI technology is the most promising method to analyse the joint, but it is expensive and time consuming to be standardized;
3. The CT scan is cheap and allows good analysis of articular cartilage and subchondral bone quality, but it is limited by the radiation exposure.

In general, these 3D methods are promising, but none presents yet a classification method to help hand surgeons grade the stage of the disease and apply the correspondent treatment, which enforces and motivates the scope of this dissertation.

2.3 Bone morphology and OA

The relation between bone morphology and OA is going to be the focus of this thesis. In this subsection the research concerning this topic is displayed. Studies based on bone morphology and their conclusions are exposed. Furthermore, the method used to conduct the study of bone morphology is explained.

The study of bone morphology was done to understand the demographic distributions of first CMC-OA. According to Halilaj *et al.* (2014), although there were no differences in bone morphology between healthy men and women, there were differences related to age. This could mean that CMC-OA high prevalence in older people could be linked with changes in bone morphology. The relation between gender, OA development and morphology remains uncertain. While Halilaj *et al.* (2014) reached the conclusion that there were no differences between bone morphology in healthy men and women. Halilaj *et al.* (2015b) carried out an analysis of joint space regarding size and showed that aging in women may lead to joint space narrowing patterns that precede early OA. Further research is required to understand the impact of gender and age in bone morphology. The ethnicity is also important to investigate, as the prevalence of CMC-OA is higher in white population and lower in Asian. Furthermore, there was an evidence that the articular surfaces of the first CMC joint were shallower in the Asian population, which led to the study of the curvature of these surfaces. From that study, the European population presented a tendency towards higher mean dorsovolar curvature of both metacarpal and trapezium, which could be linked to the development of OA (Halilaj et al., 2015). Studying the shape of the bones involved in the first CMC joint is an essential tool to understand the mechanism underlying this condition, as well as to try to predict it. The methods available to study bone morphology often relies on SSM, this method allows the easy analysis of a big dataset.

2.3.1 Statistical shape modelling

SSM is a very useful technique with many applications. This method is used in this thesis to assess bone morphology through shape analysis. Therefore, as this is going to be the most discussed field of application, it is important to understand this method.

The SSM was developed by Cootes *et al.* (1995), it is a statistical model that studies the shape of objects/structures. Given a set of structures, the model iteratively deforms to fit an example of the object. Afterwards, a statistical analysis is performed and as outputs the following are generated: the mean geometry of a shape, and statistical modes of geometric variation are inferred from a set of shapes. In this model the shapes are constrained by the Point Distribution Model (PDM).

SSM was a technological progress since it started including the variability to the mean model without losing specificity. This allows the inclusion of structures in which the shape is non-standardised. This method is mostly used in imaging, e.g. for detecting structures for segmentation. The application of this technique allows the structure to be detected, even though size or shape

variations may exist, due to disease, age, length or weight, overcoming shape dependence limitations of previous methods (Cootes *et al.*, 1995).

To facilitate the understanding of SSM an example, shown in Figure 6, is described. Let us consider that SSM is going to be applied to a dataset of hand figures. Figure 6 illustrates the landmarks distributed in specific characteristic points that define the hand shape. The landmark points define key features shared between every sample structure. Every sample would be marked in the same way, being the tip of the thumb always landmarked as number one, to allow posterior comparison.

SSM relies on the assumption that every object is composed of a set of points and a dataset of samples needs to be created. All samples from the dataset must have the same number of landmark points and be distributed in the same order to allow comparison. Calculating the distance between the respective landmark points in each sample of the training dataset allows the creation of an average model and the possible variations of these models, allowing variability. Having in mind that it is this set of statistical points that define the model, important adjustments have to be done prior to making the model, including alignment, scaling, translation and rotation, in order to obtain only the variations of the shape (Cootes *et al.*, 1995).

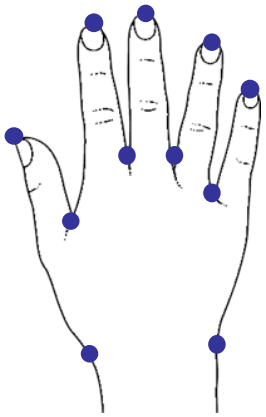

Figure 6 – Example of landmark points, marked blue, distributed in the hand shape.

Finally, techniques to reduce dimensionality such as Principal Component Analysis (PCA) are applied. PCA is a multivariate statistical, used to find patterns in the data. This is achieved by computing the covariance matrix among the structures studied. From the covariance matrix the eigenvectors, that translate the main directions and the eigenvalue, a magnitude coefficient attached to the eigenvector are attained. PCA relies on orthogonal transformation, according to the eigenvectors, to convert a set of observations of possible related variables into a set of values of linearly uncorrelated variables, called principal components. Ending up with the same number of principal components (PC) as inputs, this transformation occurs in such a way that the initial principal components have bigger variance and, gradually, the following PC variance decreases and tend to the same value (Groth *et al.*, 2013). This is a key feature, since it is only necessary to analyse the PC, also known as modes, that exhibit wide variance. The modes usually analysed, are the ones comprising 90% of the cumulative variance. Although this represents a big percentage, the total number of modes that require analysis is small in

comparison to the number of samples in the input since the first mode is responsible for 50% to 70% of the variance.

2.3.2 Bone morphology using SSM

Previous studies have already shown that statistical shape modelling (SSM) could be useful to predict or identify OA early in different joints, like the hip and knee (Gregory *et al.*, 2007; Neogi *et al.*, 2013). Although no morphological and shape factors have been established to predict or detect early OA on the first CMC joint, several studies have addressed this subject. Studies based on 2D radiographies of the joint shape were able to offer a perspective of the variance and shape of the joint but were not capable of showing the complexity involved in the actual 3D joint. The research involving the 3D structure of the joint, initially, focused in the joint's articulated surface (Halilaj *et al.*, 2014). Despite osteoarthrosis being localized on the articulated surfaces of the joint, there is evidence supporting that the entire bone should be analysed. Recent studies evaluating CMC-OA using SSM and the bone's entire shape concluded that there are changes in bone morphology in people with early OA (Schneider *et al.*, 2018).

The research on CMC-OA based on morphology, using SSM, has been helpful to understand the impact that OA has on the bone's morphology. Moreover, it allowed the understanding of the relation between shape and gender, age or ethnicity. By studying subjects with early OA, Ladd (2018) found that aging and OA affect the articular shape of the CMC joint. Furthermore, the shape is not correlated with higher incidence of CMC-OA in healthy women (Halilaj *et al.*, 2014). Using SSM in the study of shape could enlighten the scientific community about the causes of OA and explain its incidence, revealing it as a tool in the moment of treatment and prevention.

The utilization of SSM enables the easy analysis of a big data set, generating a model that includes the morphologic variations within the subjects of a given dataset. This technique reduces time consumption. Moreover, it allows the easy identification of bone regions where there is wider variation. The SSM that is used in this work is a novel method, called multi-object SSM, which allows the analysis of the two bones of the CMC joint together (Rusli & Kedgley, 2019). This is particularly interesting because the models show the two correspondent articulated surfaces and the study of the impact of OA on the trapezium and first metacarpal is more accurate.

2.4 Benefits of osteoarthrosis early detection

OA is a condition that takes decades to develop. Usually, it is only detected in the late stage of the disease, when there are already permanent changes in the joint (Chu *et al.*, 2012). Although therapy in the late stages is standardized, it has high costs associated and does not give back full mobility to the patient. Thus, an earlier detection or slowing down its development would have a very positive impact on people's lives and possibly reduce the final treatment costs. Detection of the changes

associated with the onset of OA, besides prevention, may allow clinicians to have the best chance of reducing the impact of the disease by providing alternative treatment options. Understanding the disease process, identifying potential disease-modifying treatments and evaluating the effectiveness of new therapies.

OA is treated depending on the joint characteristics. Particularly, the treatment for first CMC joint can be conservative, consisting in analgesics, joint protection, strengthening exercises of the intrinsic and extrinsic muscles of the thumb, assistive devices, and splinting, or surgical, to relieve the pain (Egan & Brousseau, 2007).The early detection of this condition enables a more aggressive prevention, such as, splinting or strengthening exercises. More investigation needs to be done in order to prove the efficacy of these methods to prevent or stop the progression of CMC-OA. This elevates the purpose of this study.

2.5 Contributions of the work

The present work is a continuation of a PhD thesis combined with the utilization of a dataset provided by a research group from Brown University. In the PhD research, a multi-object SSM model was developed to analyse the first CMC joint shape and its variation within a given population. Beyond the model, a methodology to assess and quantify the variations given by SSM was established. Considering the application of this methodology here, the present work validates the application of the multi-object SSM model developed for the evaluation of the CMC joint shape and its possible relationship with OA.

The dataset provided contained information regarding the first CMC-OA stage and the respective CT scans of a set of patients. Given the dataset features, three populations that had been evaluated in two moments in time were possible to be grouped. This allowed comparing healthy (stage 0 OA), stabilised (stage I OA) and progressive (form stage I to stage II OA) populations over time.

The main novelty of this work resides in the measurement of morphological parameters while comparing healthy and pathological populations. Concerning this matter, only qualitative research had been performed (Schneider *et al.*, 2018). The parameters measured were the tilt and torsion angle in the first metacarpal and the width and length in the trapezium articulated surface. The work developed in this thesis showed that the tilt angle in the first metacarpal was significantly different between the healthy and stabilised populations, which may be the beginning of a new diagnostic tool. Further research needs to be done to confirm if it is also a predictor. Nevertheless, this parameter was found to be able to detect early stage OA.

3. METHODOLOGY

The methodology followed in this work is divided into two parts, as illustrated in Figure 7. The first part comprises the methods used to obtain the results. Briefly, from a large CT dataset, 6 groups were defined according to their OA condition and evolution, over a time period. After ensuring a proper definition of the segmentation models, statistical shape models were applied, which allowed the 6 groups to be defined by a set of principal components. In the second stage, methods were used to allow the analysis of each population principal components, two comparisons were made. Initially, the relevant PCs for each group were found. A qualitative analysis was performed, characterizing each population. Moreover, different populations were overlapped and compared using distance map that displays the difference in millimetres. And a quantitative comparison, where the first CMC joint morphological parameters, tilt angle, torsion angle, length and width were measured and its differences among populations statistically analysed. The following sections provide further detail on the methods applied.

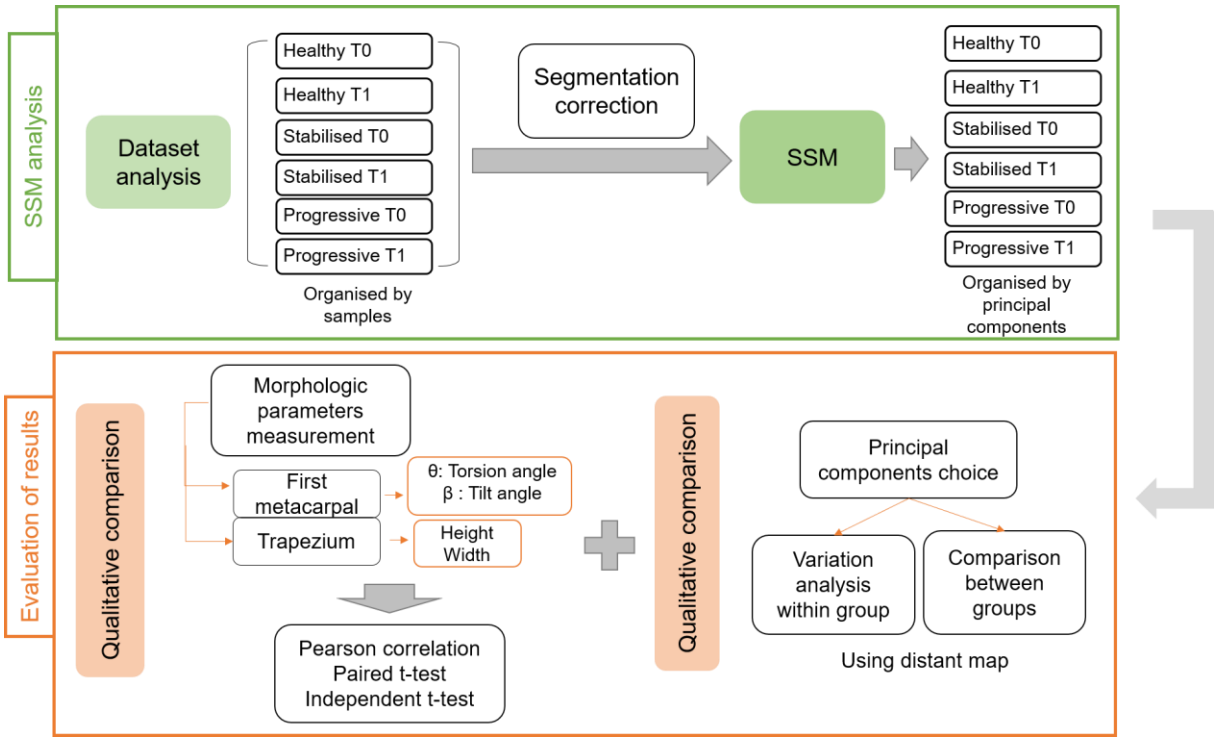

Figure 7 – Scheme showing the major steps followed in this work. The first part, in green, denotes the processing of data until the acquisition of statistical analysis data, while the second part, in orange, denotes the procedures performed for the evaluation of the results.

3.1 Dataset description

The dataset used was provided by a research group from Brown University (Halilaj *et al.*, 2014) who made a comprehensive study to analyse the development of OA in the first CMC joint throughout time. This study was meant to provide a broader understanding about CMC-OA. The imaging techniques and dataset characteristics defined when the study was made are described next.

All subjects were imaged with a 16-slice clinical Computed Tomography (CT) scanner (GE LightSpeed 16, General Electric, Milwaukee, WI) with the following scanner settings: tube parameters at 80 kVp and 80 mA, slice thickness of 0.625 mm, and in-plane resolution of at least 0.4 mm x 0.4 mm. The imaging technique performed provided a 3D image of the hand. From the CT data, thirteen hand bones can be distinguished, amongst other tissues. After CT scanning, all subjects performed a radiography for the acquisition of 2D images. The protocol followed positioned the hand in such a way that the sesamoid bones were superimposed on one another.

The subjects were followed up for 6 years. All subjects were asked to have baseline CT in the beginning of the study. The protocol also included four more CT scans at one year and half, three years, four years and half, and six years later. All subjects had two CT scans from different moments in time, the first being the baseline. All subjects were diagnosed regarding first CMC-OA. The 2D radiography was evaluated by a board certified orthopaedic hand surgeon according to the Eaton-Littler classification (Eaton *et al.*, 1984). This classification varies from 0 to IV, where 0 corresponds to a healthy subject an IV to a severe case of OA. The asymptomatic subjects were re-examined to ensure that they had no prior conditions that might have altered CMC joint morphology. The dataset also included parametric information, such as age, height, weight and gender.

3.2 Selection of subjects

The selection of subjects to be analysed in the present study followed three criteria considering the aim of having different populations evaluated over time. Each group had to have more than twenty subjects to have good representability. The subjects grouped together had to have the same OA stage in the baseline assessment and the same evolution over time. Only subjects diagnosed with stage 0, I and II were considered, this criterion was defined since it is easier to analyse less damaged bones. Furthermore, if a correlation between shape and OA development can be made on early stage OA, shape correlation is likely to exist as well on advanced stage OA.

Among the selected subjects, some were healthy at the beginning, some already had OA. In the end, some subjects remained healthy or maintained their OA level, whereas others worsened throughout time. In order to find the morphologic variations in the first CMC joint associated to OA, it was necessary to select which data was meaningful to be analysed. From the 95 subjects in the dataset,

three populations were formed: healthy, stabilised and progressive. The dataset allowed the progression study of OA since it contained at least two CT scans of every subject at different moments in time. An initial time (T0) was established at baseline and final time (T1) one year and half or six years later. Given that the present study was mainly focused on the subjects OA stage, the amount of time between observations was not considered. Therefore, although three populations were defined, each population comprised two groups (T0 and T1), resulting in a total of six groups that were analysed.

The healthy population was composed of subjects that were asymptomatic in the initial (T0) and final moments (T1). It comprised 22 subjects, 8 and 14 of which were male and female, respectively. This population was the control group, since it allowed to perceive the normal joint shape. The stabilised population included subjects with stage I CMC-OA at T0 that did not evolve at T1. This population had 27 subjects, from which 13 were males and 14 were females. The final group, denoted as progressive population, included subjects whose CMC-OA stage evolved from type I to type II. This group comprised 36 subjects, 19 males and 17 females. Both stabilised and progressive populations are pathological.

Table 1 characterizes the three populations in both moments of time, according to age, BMI, the number of subjects and female percentage. It is noteworthy that the healthy population is younger when compared to the pathological populations. Moreover, the progressive population exhibited higher BMI.

Table 1 – Description of the six groups analysed. The number of subjects and female percentage of each population is presented. Age and BMI are described regarding range and average (Av.) for each group.

		Number of subjects	**Age [years]**	**BMI**
Healthy	*T0*	22 (63.6% female)	23-75 (Av 52.95)	18-43.9 (Av. 25.48)
	T1		29-81 (Av 57.95)	18-36.5 (Av. 25.89)
Stabilised	*T0*	27 (51.8% female)	47-72 (Av 58.26)	17.8-38.4 (Av. 25.86)
	T1		49-74 (Av 61.07)	17.8-40.2 (Av. 26)
Progressive	*T0*	36 (47.2% female)	45-75 (Av 59.39)	20.4-38 (Av. 28.1)
	T1		47-77 (Av 62.11)	20.4-42.8 (Av. 29.1)

3.3 CT data segmentation

After choosing the group of subjects that are going to be analysed, the focus became the processing of the CT data. The hand CT scans were already segmented using the software *Mimics (v.17, Materialise,*

Belgium) and contained all hand bones in separate files. Left hands were mirrored to the right hand so that all files were displayed in the same orientation. Although the data given comprised thirteen hand bones, only the first metacarpal and trapezium were relevant for the present study. Yet, due to its proximity and possible interest of study in advanced cases of OA, the scaphoid a bone close to the trapezium, also underwent the process of correction for post segmentation errors.

The CT scans were automatically segmented. The automatization of this process decreases time consumption while guaranteeing the same accuracy in a large number of cases (Sharma & Aggarwal, 2010). This method can be applied using several approaches, but usually it relies on the intensity difference among tissues to segment. However, CT scans have artefacts due to the acquisition method, which make the process of automated segmentation harder. Intensity inhomogeneities and the partial volume effect are also obstacles to the technique. After segmentation, the surfaces of the structures commonly show signs of pixelization and/or small incongruences. These details are concerning aspects when performing a shape analysis. Consequently, they must be addressed.

The correction of post segmentation errors is a key step since it smoothens the surfaces and corrects segmentation inaccuracies, allowing a sounder statistical shape analysis (Liu, Dong & Peng, 2010). The software *Geomagic Studio 12 (Raindrop Geomagic, Research Triangle Park, NC, USA)* was used for this purpose. Three tools from this software were used, namely the *Reduce noise, Relax polygons* and *Mesh Doctor.* These tools have different levels of strength that were chosen after a careful analysis. After application of each tool, the variation in shape could be observed, allowing the evaluation of which level performed better in smoothing the surface without removing the characteristic features in each shape.

The first operation was meant to reduce noise. Thus, it eliminated points in flat regions but preserved points in high-curvature regions to maintain detail. Several degrees of intensity were possible to be set. Different levels were tested, as illustrated in Figure 8. The tests were done in the first metacarpal since its larger surface allowed an easier identification of differences. When the strength of the tool *Reduce noise* was increased, the areas affected were wider and more severely deviated. For this reason, the strength level one was deemed as best to preserve the bone morphology.

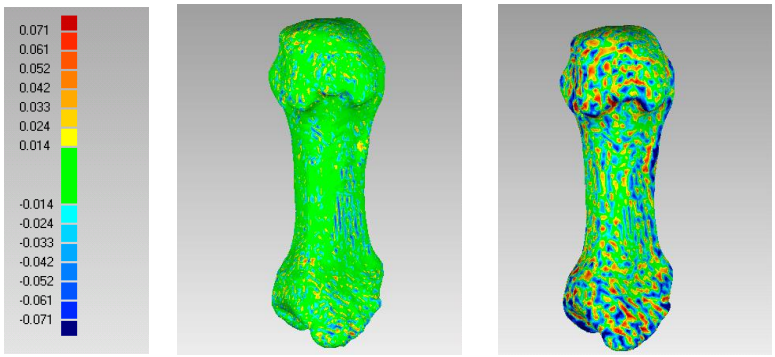

(a) (b)

Figure 8 – Deviation in millimetres when applying the function Reduce Noise. (a) strength level 1. (b) strength level 3.

The tool *Relax polygons* comprises three parameters, namely smoothness level, strength and curvature priority, which mainly conduct the smoothing and optimization of the polygon mesh data surface to improve the quality of the bone surface, correcting mainly edgy points that arise from segmentation. These three features are connected. Smoothness level accounts for the smoothing of the surface, a higher smoothness level would detect smaller spikes. The strength defines the intensity in which these spikes, already detected, are smoothen. The higher the strength, the more it smoothens a spike. Lastly, curvature priority, accounts for not losing detail, which is critical in this work. To evaluate the influence of each parameter on bone morphology, different tests were performed in which two parameters were left constant and only one was changed. Default values of smoothness were used, but curvature priority was maximized in order to maintain the curvature of the geometry. Strength had a large influence on the overall smoothing and was minimized in all cases so that the volume of the geometries changed less than 1%. The effects of altering the parameters of the *Relax polygons* tool are displayed in Figure 9. The best set of parameters, i.e., the set that allowed the shape to be corrected while preserving the morphology of the bone is presented in Figure 9(a).

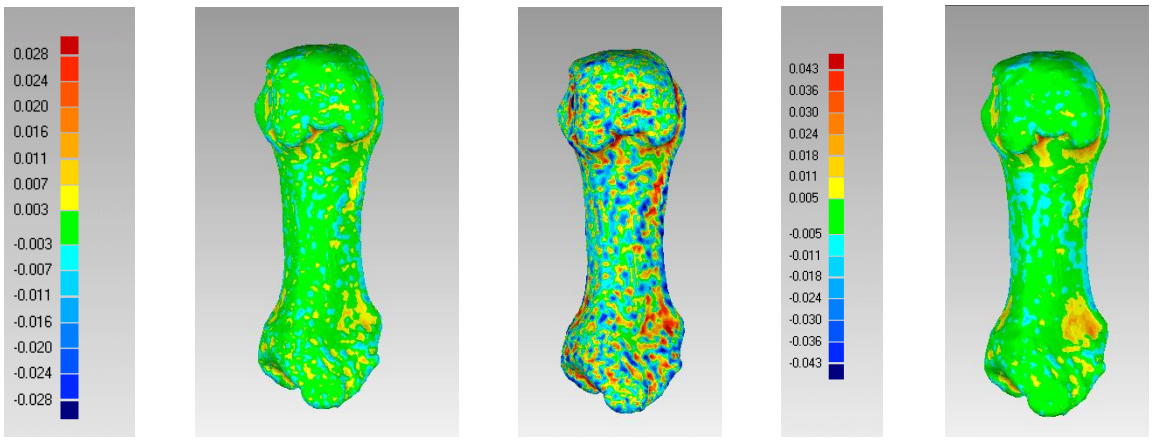

Figure 9 – Deviation in millimetres when studying the Relax polygon function. (a) smoothness level one, strength one and curvature priority four. (b) smoothness level four, strength one and curvature priority four. (c) smoothness level one, strength four and curvature priority four.

Finally, the last tool used was *Mesh doctor*, which enables the automatic reparation of defects in the mesh, improving and preventing errors on future steps. This function signalizes the following flaws: non-manifold edges, located on the objects boundary in which triangles are not connected on the two sides; Self-intersections in which triangles are tangled or intertwined with other neighbouring triangles; Highly creased edges, when the edges curvature is to prominent; Surface spikes, when triangles are organised forming little pyramids on the surface; Small components, characterized by free-standing triangles that are few in number and represent noise; Small tunnels, double-layered triangles in the mesh with a front and back opening; and small holes.

When applying this function, all features were selected to be detected and solved, except for small tunnels. The software alerts the user by highlighting in red the locations of the defects, as displayed in Figure 10. It also specifies the type of each defect and allows the user to automatically correct it.

After setting the right parameter levels, the first metacarpal, trapezium and scaphoid of all subjects in the dataset were corrected following the same protocol.

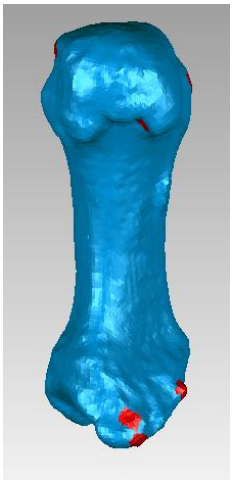

Figure 10 – Function Mesh Doctor, signalizing defects on the mesh. In this example 58 spikes were detected.,

3.4 Statistical shape modelling

Having the samples corrected, the six groups were run by SSM. The multi-object SSM performed in this work was developed in-house by Wan Rusli (Rusli & Kedgley, 2019) in *Matlab* (R2016B, Mathworks, Natick MA, USA) and in *RStudio*. This method is split into two parts, described in detail in Sections 3.4.1 and 3.4.2. The first part enables the understanding about the alignment and registration process that altogether allowed point comparison among samples. The second part consists in a statistical method, PCA, which allows the down-sampling and creation of variation models. Section 3.4.3 provides a brief description regarding the implementation of the statistical shape modelling method applied.

3.4.1 Rigid and non-rigid registration

Rigid and non-rigid registrations were employed in order to achieve the alignment of all the samples being compared. This is accomplished by placing all the samples in the same space and orientation. On one hand, rigid registration is used when objects only need to be rotated and translated with respect to one another to achieve correspondence. On the other hand, non-rigid registration is used when the correspondence between structures in two images cannot be achieved without some localized stretching of the images (Crum, Hartkens & Hill, 2004). Both were used in this work by applying a set of algorithms. In addition, sub-sampling was also performed in order to decrease the computational time.

The rigid registration of all bone structures within a given population was achieved using the rigid coherent point drift (CPD) algorithm (Myronenko & Song, 2010). The goal of CPD is to assign correspondences between two sets of points and/or to recover the transformation that maps one-point set to the other. This is attained through the alignment of two-point sets as a probability density estimation, in which one-point set represents the Gaussian Mixture Model (GMM) centroids and the other represents the data points. Iteratively, the GMM centroids are fitted to the data by maximizing its likelihood. In addition, the GMM centroids move coherently as a group, which preserves their topological structure (Myronenko & Song, 2010). Registration is, therefore, needed to place the data into a common reference frame by estimating the transformations between the datasets (Fitzgibbon, 2003).

Subsequently, all samples were sub-sampled using the relevance-based sampling algorithm (Rodolà *et al.*, 2015). The main goal of the relevance-based sampling algorithm is to select surface points that are relevant with respect to the task to be performed. The relevance of a point is assessed based on how similar the points around it are. The similarity between points was based on what is described in the work of Rodolà *et al.* (2015). In the end, only the relevant points are kept. The down-sampling of the 3D model of the first CMC was achieved by retaining high density points on specific regions (Rodolà *et al.*, 2015). Then, non-rigid registration is performed using the CPD algorithm (Myronenko & Song, 2010), in the sub-sampled dataset. This task is named coarse non-rigid registration and allows to obtain the initial point-to-point correspondences.

Given that the dataset is subsampled, a fine non-rigid registration was executed, employing the original dataset (which contains all points), which allows to improve the accuracy of the non-rigid registration. This was made based on a local optimization algorithm (Li et al., 2008) to preserve local structure during the deformation of the target object to the source object. By using the original samples during the local optimisation, the effect of sub-sampling during the coarse non-rigid registration process is eliminated.

Following these steps, the output files contain the two bones, trapezium and first metacarpal, aligned and scaled. Along with the files described, the shape vector, which describes the coordinates of the landmark points of each subject, is also generated. The shape vector presents 3N columns, being N the number of points of each joint and M lines, being M the total number of samples in a group. This file is the input for the next step consisting in a principal component analysis.

3.4.2 Projection pursuit Principal Component Analysis

After obtaining all samples aligned, a statistical method needs to be applied in order to analyse the differences between samples. The method used is the projection pursuit principal component analysis (ppPCA), a robust method that is more resistant to outliers than usual PCA methods (Croux, Filzmoser & Oliveira, 2007). Outliers are the points that are incorrectly extracted from the image and have no correspondence in the other point set. Projection–pursuit (PP) methods aim to find structures in multivariate data by projecting them onto a lower-dimensional subspace. They are characterized by the reduction in the shape vector dimensionality. The ppPCA was implemented in *RStudio*, since Croux,

Filzmoser & Oliveira (2007) provided the library for this algorithm in R. Having the shape vector as an input, ppPCA was performed. Operating with this method allows the creation of models that display the variance present on the input samples shape, based on the shape vector. As output, the ppPCA generates eigenvectors, which account for the directions in which there are larger point concentrations, eigenvalues, which quantify the variance in each eigenvector, and PC scores, which are a classification of the variance present in each model.

Using the software *MATLAB*, the mean model, that corresponds to the average all sample points from each subject contained in the shape vector, was computed. The PCs are generated according to equation (1), adapted from Rusli & Kedgley, (2019):

$$x_{ik} = \bar{x} + k\sqrt{\lambda_i}\varphi_i \quad (1)$$

where $\bar{x}$ represents the mean model and φ_i represents the $i-th$ eigenvector that varies between $1 < i < M$, where M is the number of samples inserted on the PCA. The term $k\sqrt{\lambda_i}$ is the weighing factor, in which λ_i represents the eigenvalue that translates the variance and the square root of variance ($\sqrt{\lambda_i}$) is the standard deviation. By multiplying $\sqrt{\lambda_i}$ by k the user can assess a wide range of variation. Considering normal distribution, k is usually set to $-2 \leq k \leq 2$ to obtain a confidence interval of 95%. Therefore, the variance present in each PC should vary linearly with k.

3.4.3 Application

The pipeline followed for the application of the SSM model is depicted in Figure 11. Firstly, note that all the 6 groups were run individually. From each group a reference sample was selected to perform the alignment described in Section 3.4.1. This choice was based the quality of the segmentation. A subject was chosen from each population. The same subject served as reference in T0 and T1 using the respective sample.

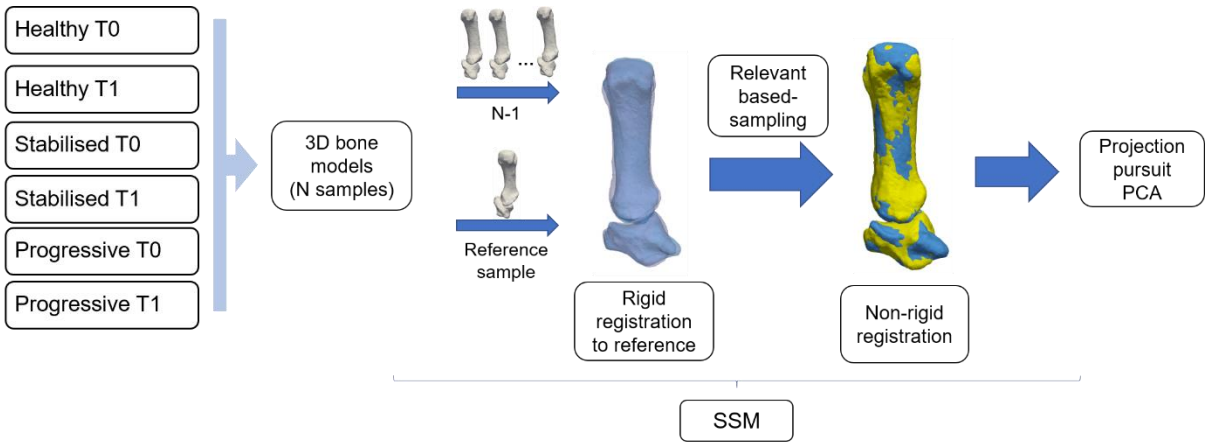

Figure 11 – Scheme showing the implementation and pipeline of SSM. As input there are six groups that were run individually. The output arises from ppPCA. Adapted from (Rusli & Kedgley, 2019)

Following the scheme in Figure 11, the samples were registered and scaled, since size differences are not morphologically relevant and could mislead the results, scaling of the remaining samples to the reference model was performed. Before the ppPCA application, the relevance base sampling, non-rigid registration and local optimization, previously explained, were performed. As output each group, besides the mean model, is composed of as many PCs as M samples and each PC gathers 4 standard deviations, according to Equation (1).

3.5 Evaluation of the results

The following subsection describes the methods used for the analysis of the results. From this section on, the goal is to analyse the outputs of SSM. Two approaches were conducted, a qualitative one, in which the global bone shape within and between groups was compared. And a quantitative approach, in which morphologic parameters of the first CMC were defined, measured and statistically analysed. Both analyses were achieved using the software *Materialise 3-matic.* This software was developed specially to analyse anatomical shapes, maintaining sufficient detail and allowing working directly on triangulated surfaces.

The aim of both approaches was to detect differences between healthy and pathologic populations.

3.5.1 Qualitative comparison

Qualitative comparison is characterized by the comparison between two bone models, assessing its differences in a qualitative way. This analysis is meant to oversee the morphologic changes of the bone shapes. Primarily, it is necessary to assess the number of PCs that are relevant to the analysis. Afterwards, the characterization of each population was achieved, and finally comparisons between groups were made to understood if there were differences between populations.

The output of SSM are the PCs. As mentioned in Section 2.3.1, the analysis should occur in initial PCs that assemble the variation majority. Usually the number of PCs analysed considers 90% of cumulative variance (Schreiber *et al.*, 2018; Groth *et al.*, 2013). However, since non-rigid registration and scaling were performed, less variation exists. According to Van De Giessen *et al.* (2009), only the modes that have variance above 5% should be taken into consideration and analysed in such cases. Therefore, the first step was to assess the number of PCs relevant for the analysis in each group.

Subsequently, the characterization of each population was achieved using the T0 group, by evaluating the variance present in the correspondent PCs. This analysis was made to each population using the PCs found relevant. Besides the number of PCs, the variation of each PC needs to be defined, during this analysis $-2 \leq k \leq 2$ was considered. For each population, the comparison was performed between the mean model and each PC's positive and negative SD, allowing to visualise the range of variation of each mode. The tool employed for this analysis was *Create part comparison analysis*, which permits the direct comparison between two samples given the deviation between the meshes of two

structures. The results were exhibited using a colour grid exhibiting deviation distances in millimetres. This enables the user's fast perception of the bone regions that vary when compared to another model.

Direct comparison within the healthy, stabilised and progressive populations between T0 and T1 groups was also necessary. This was achieved by comparing directly the mean models of each two groups with the function *Create part comparison analysis*. Because these models were not aligned, the protocol described in Section 3.4.1, rigid registration, was applied to ensure that the mean models were aligned. This comparison is interesting to find if the groups that progress into OA exhibit different patterns when compared to the healthy group.

Finally, a comparison between the healthy, stabilised and progressive groups was performed to evaluate how shape differs directly. This analysis is relevant when the stabilised T0 group and progressive T0 group are compared since the OA stage in these two groups is the same, particularly stage I. However, at T1 the progressive population evolved to stage II, whereas the stabilised population maintained stage I OA. The comparison between progressive T0 and stabilised T1 was also carried out. In addition, the analysis between healthy and stabilised (pathological) populations was also carried out. To corroborate the hypothesis that OA development in the first CMC joint is linked with the bone morphology of the joint, variance is expected to be found in these two specific cases.

3.5.2 Measurement of morphologic parameters

The measurement of morphologic parameters allows quantifying bone shapes and making comparisons between groups that have different characteristics. These measurements were done using *Materialise 3-matic* software. To measure these parameters, each bone of the first CMC joint, first metacarpal and trapezium, followed a different protocol (Rusli & Kedgley, 2019), due to their different bone morphology.

It is also important to state that the samples that were analysed in each group were the mean and the first two PCs. In each PC, the variation was considered setting $-2 \leq k \leq 2$, thus, besides the mean, four more models were assessed (-2SD, -SD, SD and 2SD). The SD models were analysed to guarantee an analysis of a wide range of variation in each PC. Moreover, it also allows the validation of the linear relation of the morphologic parameters measured in the SD models. Regardless of the number of modes that were found relevant to be analysed, the measurement of the morphological parameters was only carried on the first two modes of each population because, from the third mode on, the articulating surfaces exhibited lack of definition, especially on the borders' surface, amongst others details that altered its usual shape. This made the protocol unpracticable from the third PC on. This was more prevalent on the populations that already suffered from OA, who presented more modifications in shape. However, for sake of consistency, the same procedure was applied in all groups.

The protocol followed for each bone is detailed next.

- **First Metacarpal**

The morphological parameters measured on the first metacarpal were the tilt angle and torsion angle, illustrated in Figure 12. The tilt angle, β, translates the way the first metacarpal is rotated along the YZ

plane, while the torsion angle, $\theta = 90 - \sigma$, translates its rotation in the XZ plane. These parameters were chosen according to Rusli & Kedgley, (2019) . The tilt angle is an indicator of the volar rotation, which has been linked with OA development before (Kovler *et al.*, 2004).

To measure these angles, a coordinate system was firstly created according to ISB recommendations (Wu *et al.*, 2005).

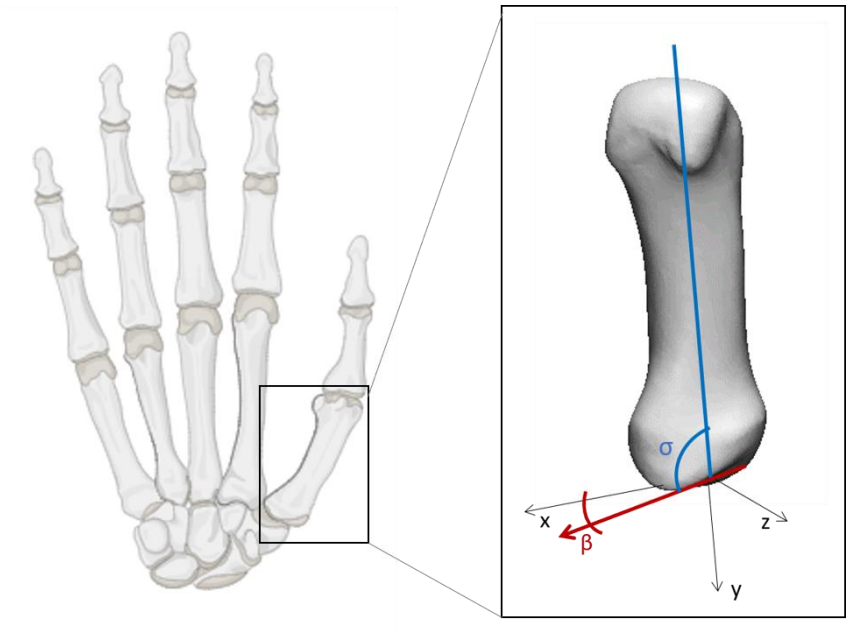

Figure 12 – Illustration of the morphological parameters measured on the first metacarpal. The tilt angle θ=90-σ is represented in blue and the torsion angle β is represented in red.

These state that the origin for each of these coordinate systems is located midway between the base and head of each metacarpal, approximately in the centre of the tubular bone. The Y axis is defined as the line parallel to a line from the centre of the distal head of the metacarpal to the midpoint of the base of the metacarpal. The X and Y axes form a sagittal plane that splits the metacarpal into mirror images. Finally, the Z axis is the common line perpendicular to the X and Y axes. This process is shown in Figure 13.

When creating the system of coordinates, the first axis generated was the Y axis. The aim was to have the Y axis longitudinal to the bone and passing through the centre of the articular surface and the middle point of the first metacarpal's head. Firstly, the middle point of the first metacarpal's head and base was identified. To define the middle base point, the articulating surface was delimited and clipped. This was achieved with the tool *Lasso Area Mark*. The coordinators of the middle point of this surface were obtained through the visualization in *CloudCompare*. Once the coordinates of the centre point were identified, they were introduced in *Materialise 3-matic*. Figure 13(a) illustrates the centre point of the articulating surface of the first metacarpal, coloured blue. The middle point on the head was defined as the middle point between the two most salient points of the head's metacarpal. These points are called condyles and are marked in red in Figure 13(a), in which the middle point is coloured orange.

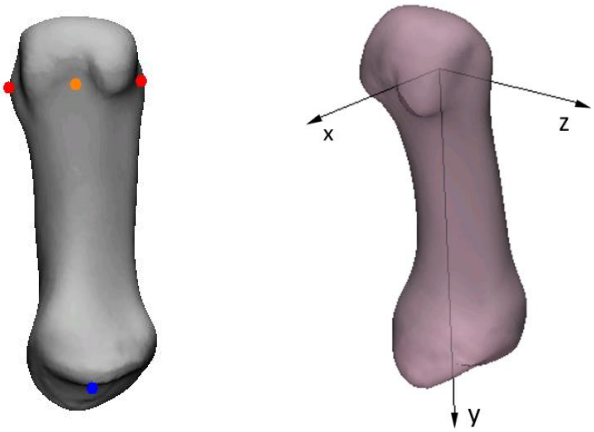

(a) (b)

Figure 13 – First metacarpal bone: (a) Points considered for the definition of the Y axis of the coordinate system of the first metacarpal. The most inferior point, in blue, is the base centre point. The orange point is the head centre point. The red points are the condyles. (b) coordinated system, aligned with the coordinated system created.

The Y axis was defined from the middle point of the head to the middle point of the articulated surface, as depicted in Figure 13(b).

The X axis was created such that the X and Y axes form the sagittal plane. To achieve this, an auxiliary plane was created considering the middle point of the head, the more rounded condyle and the centre point of the base of the first metacarpal. The X axis, as illustrated in Figure 13(b), is a line perpendicular to the created auxiliary plane.

The Z axis was computed by the cross product between the X and Y axes.

Before being able to compute the angles, the coordinate system generated had to be aligned with the coordinate system of the software 3-matic, since angles were measured according to these axes. This was achieved using the tool *measure angle* and *rotation.* The tilt and torsion angles were measured by defining a line that connects the sharpest points, the dorsal and volar cusps, on the first metacarpal articulated surface, as illustrated in

Figure 14.

Figure 14 – Base of the first metacarpal bone highlighting articulated surface. Line between the dorsal and volar cups of the articulated surface, coloured in red, to measure the tilt and torsion angle.

To help visualize the sharpest points, a curvature analysis, using the tools available in the software *3-Matic,* was performed. This analysis allowed to visualize the areas with a wider curvature using a colour grid.

In Figure 15, the angles measurement done in the software is displayed. It is possible to observe that the tilt, Figure 15(a), was measured between the line in red and Y axis, rotated along the XY plane. The torsion angle, Figure 15(b), was measured between the red line and X axis, and it was rotated along the XZ plane.

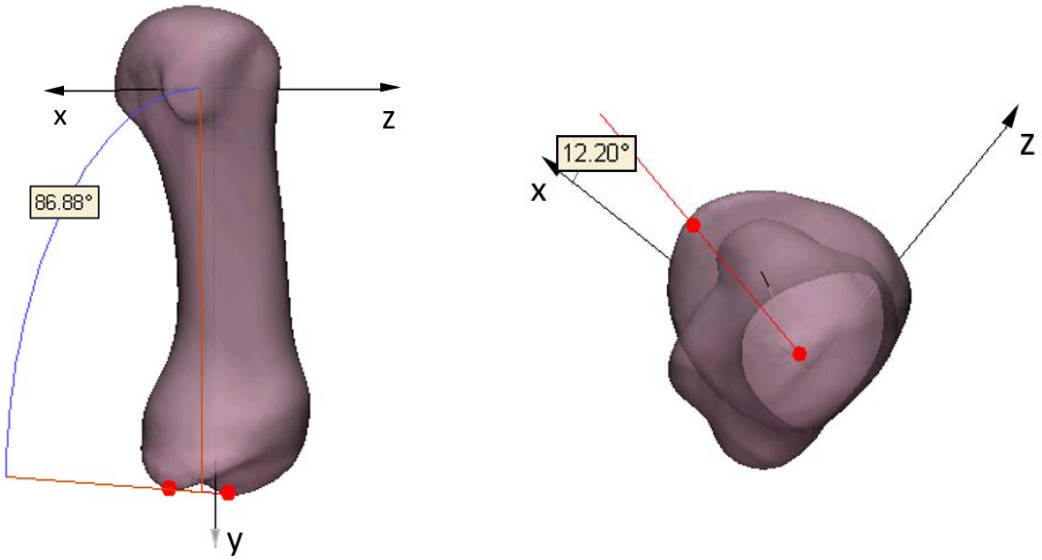

(a) (b)

Figure 15 – First metacarpal bone exhibiting the measured angles: (a) tilt angle and (b) torsion angle on the XZ plane.

- **Trapezium**

The morphological parameters that were measured on the trapezium, displayed on Figure 16, were the width and length of the articulated surface of the first CMC joint, these parameters were defined to assess how the articular surface area varies.

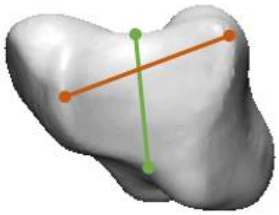

Figure 16 – Illustration of the morphological parameters measured on the trapezium. The width and length are represented in orange and green, respectively.

The width, marked in orange in Figure 16, is the distance between the sharpest points of the articulated surface, while the length, coloured in green in the Figure 16, is the distance between the depression points of the articulated surface.

3.5.3 Statistical analysis

The statistical analysis was mostly necessary when examining the measurements done. Correlation and statistical significance need to be assessed in order to take robust conclusions. The statistical analysis was performed using IBM SPSS Statistics (ver. 25 IBM Corp., Armonk, USA).

Pearson correlation coefficient was computed to verify which PC correlated the most with the measured morphologic parameters. It is important to recollect that, quantitively, only the first two PCs of each group were analysed. In each PC, the variation was evaluated from +2 SD to -2 SD considering 1 SD intervals. Accordingly, besides the mean model, four more models were evaluated, which correspond to the variations within the PC. Thus, it is expected that if the parameter is well suited to quantify variation it will vary linearly with SD. The first and second PC present different ways of variation. Therefore, the Pearson correlation coefficient was obtained between each PC (among the four parameters measured) and the trend {-2, -1, 0, 1, 2}, that described the tendency of the SD. The Pearson correlation test provides a correlation R that varies between -1 and 1. If R is in the interval $[-1,-0.7] \cup [0.7,1]$ the correlation is strong. If R is in the interval $[-0.7,-0.3] \cup [0.3,0.7]$, the correlation is only moderate, and if it is among $[-0.3,0.3]$ the correlation is negligible. Along with the R value, the statistical significance is also generated. The p-value shows how statistically strong the correlation value is. A result is usually considered statistically significant if the p-value is below 0.05 (Ross, 2012). The Pearson coefficient correlation was attained for the first and second PCs in the three populations, at T0 and T1, for each morphologic parameter. The PC that better correlates, i.e. with a higher R value, with the morphologic parameter is used in the following statistical analysis.

A paired t-test was done to understand if there were statistically significant differences in the morphologic parameters between the populations at T0 and T1. This was made using the PCs, previously chosen using the Pearson correlation coefficient. This test aimed to determine whether there was statistical evidence that the mean difference between paired observations on a particular outcome was significantly different from zero. In the present case, time was the changing variable. To apply this method, some constraints must be fulfilled: the dependent variable must be continuous, the groups being compared must be related, a random sample should be picked, and a normal distribution of the differences between the paired values must be verified. These differences should not contain outliers (Ross, 2012). The paired t-test outcome gives the paired samples statistics, correlations and the test. The last output is the most important to examine. If the paired t-test p-value is below 0.05, a statistically significant difference exists.

An independent t-test was done to quantify the statistically significant differences in morphologic parameters measured between populations (Ross, 2012). Since this test allows the comparison of two variables, the comparisons were made two by two to determine whether there is statistical evidence

that the associated population means are significantly different. The PCs used to define each group, were chosen according to the Pearson correlation coefficient, previously set. The constraints that must be assessed before performing the t-test are the following: the dependent variable must be continuous and the independent variable categorical, the groups compared should be independent form each other, the dependent variable must follow normal distribution, and there should be homogeneity of variance. The results were divided between the Levene's test for equality of variances and t-test. The last is assessed and if p-value was below 0.05, the test was considered to be statistically significantly different.

Finally, to better perceive the morphologic parameters differences and ranges between populations, charts exhibiting the three populations measurements, their mean values and standard deviations were developed.

4. RESULTS

This section presents the results obtained from the application of SSM. The results are divided into a qualitative analysis, in which the two bone shapes are compared, and a quantitative analysis, in which four parameters measured for each population are compared.

4.1 Relevant principal components to analyse

Given that the results arose from a SSM, the outputs that were examined were the PCs. The benefit of using SSM and not analysing every sample individually is the reduction in time analysis. The variance of each PC was analysed: this information was displayed graphically as shown in Figure 17.

Figure 17 presents the variance of the PCs of the progressive population at T0. Overall, 35 modes were computed. The variance percentage of each PC translates the eigenvalue magnitude of each PC. The greatest percentage of variance, exhibited by the first PC, was 12%. The second mode accounted for 6% of variance. The first twenty-seven modes accounted for 90% of the total variance. About 29% of the total variance was gathered by the first four modes, all of which presented a variance larger than 5%. As expected, the variance of each principal component decreased as the principal components increased.

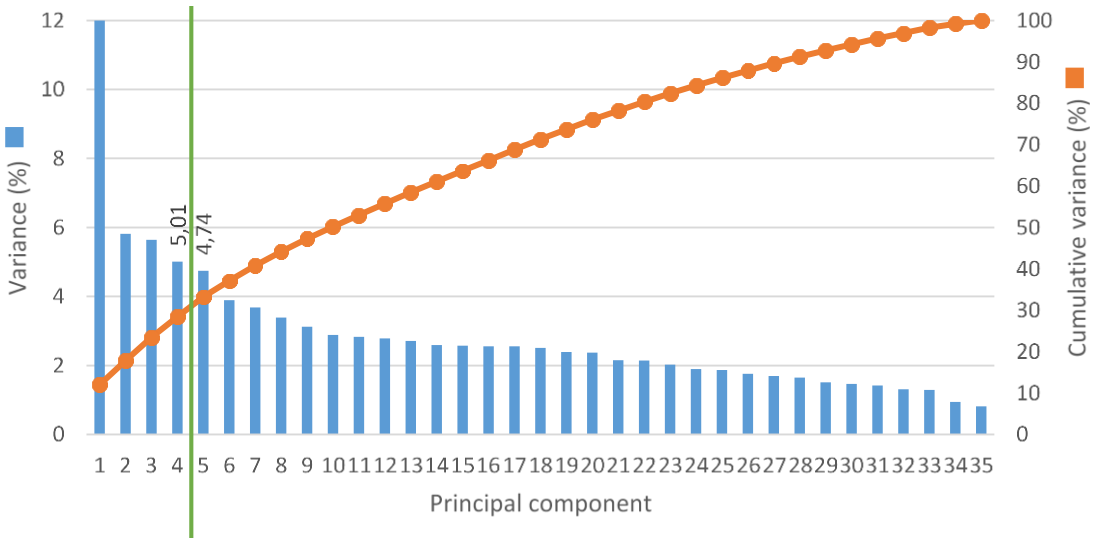

Figure 17 – Variance and cumulative variance of the progressive group at T0 explained by 35 PCs of the SSM. The green line shows the limit of being above and below 5% variance.

From the analysis of the remaining five group charts, a similar behaviour was detected for all, even though the number of modes with variance above 5% and the total variance that those modes gathered

varied. For the sake of conciseness, they are displayed in the Appendixes section A. Table 2 summarizes the most relevant data for the groups that underwent SSM, including the number of PCs with variance greater than 5%, the variation of the first PC and the variation gathered by the respective number of PCs that was relevant to analyse in each group.

Table 2 – Number of PCs relevant for analysis (variance above 5%), amount of variation for the first PC and cumulative variance of the relevant PCs, organised by group.

	Number of PCs	First PC variation	Cumulative variation of relevant PCs
Healthy T0	7	13%	53%
Healthy T1	8	13%	58%
Stabilised T0	6	10%	42%
Stabilised T1	5	13%	39%
Progressive T0	4	12%	29%
Progressive T1	4	11%	27%

4.2 Qualitative shape variation

The qualitative analysis of the shape variation is of importance since it allows understanding the overall shape variation. Although the effects of OA are present mostly on the joint, i.e., on the articulating surfaces of the first CMC joint, a strong relation between change in bone shape and OA development has been reported in the literature (Schneider *et al.*, 2018). After understanding which PCs were relevant to analyse in each group, a qualitative analysis was made in each group to understand the variations of each population. Post-hoc comparisons between populations were made to understand the differences in shape as it relates to time and joint condition.

4.2.1 Characterization of each population

Characterization of each population entails the analysis of the range and type of variation that occurs in each group. Therefore, the PCs that were defined as relevant were assessed. For each PC, the mean model was compared with -2 SD and symmetrical +2 SD models. The SD represents the square root of the eigenvalue of a PC. The results for the first metacarpal and trapezium are presented for each group. Given the extent of the analysed data, the T0 group of each population is considered to represent each population and the remaining three groups (T1) are only presented in Appendixes section B. For the first metacarpal, two views are presented, whereas for the trapezium only the articulating surface is shown. Afterwards, the two bones of the first CMC joint are analysed amongst all PC. The first

metacarpal was analysed overlooking its head, shaft, base and articulating surface. In the trapezium, the articulating surface was compared and analysed overlooking the transverse XY plane.

- **Healthy**

The healthy population did not exhibit first CMC-OA. This group comprised seven PCs, depicted in Figure 18, in which both bones of the first CMC joint are presented. Overall, variations were detected in the shape of both bones. Moreover, the first PC showed wider variation when compared with the remaining modes.

Concerning the first head of the metacarpal, and with exception of PC 4, all PC exhibited variation on the distal side. This variation, whether positive or negative, is related with the bone length increase or decrease, with stronger variation found for the first two PC. Shaft thickness variations were also detected in some of the PCs that presented length variation. As the PC shaft got longer, it became less thick and vice-versa. The PCs one, two and six are examples of this combined variation. On the palmar side of the head of the first metacarpal, there were two protuberances that concentrated variation, as shown in PCs one, three, four, six and seven. The last three PCs presented some variation in the condyles and in the extremities of the head on the ulnar and radial sides. Regarding the base of the first metacarpal, PCs one and two exhibited variation all around, meaning that there was thickening and shrinking occurring at the base. Variations on the volar beak of the base were detected in PCs five, six and seven. The articulating surface exhibited greater variation on the ulnar side. Variations in all PCs were more concentrated on the periphery, except for the third PC.

With respect to the trapezium articulating surface, variation was more concentrated on the periphery, except for PCs six and seven. By examining all PCs, it can be seen that both ulnar and radial ridges presented variation, with the radial variation being more prominent. The palmar depression presented variation in most PCs. The second and third PCs presented one of the ridges with a positive variation and the other with a negative variation.

- **Stabilised**

The stabilised population was diagnosed with stage I CMC-OA. The six PCs found relevant are displayed in Figure 19. Variations in bone shape were found to be widely spread in all PCs, especially PC one, which showed the widest variation.

Concerning the trapezium articulating surface, variation concentrated more on the periphery in all PCs besides the second PC. The ulnar and radial ridges presented variation, from the third PC onwards. The palmar depression presented variance in all PCs.

Regarding the first metacarpal, it is noteworthy that the stabilised population exhibited more marked variation, mostly in the shaft, compared to the healthy population. The variations in the shaft occurred mostly in the ulnar and radial sides, as shown in the first, third and fourth PCs. However, there are also PCs that presented variation all around the shaft.

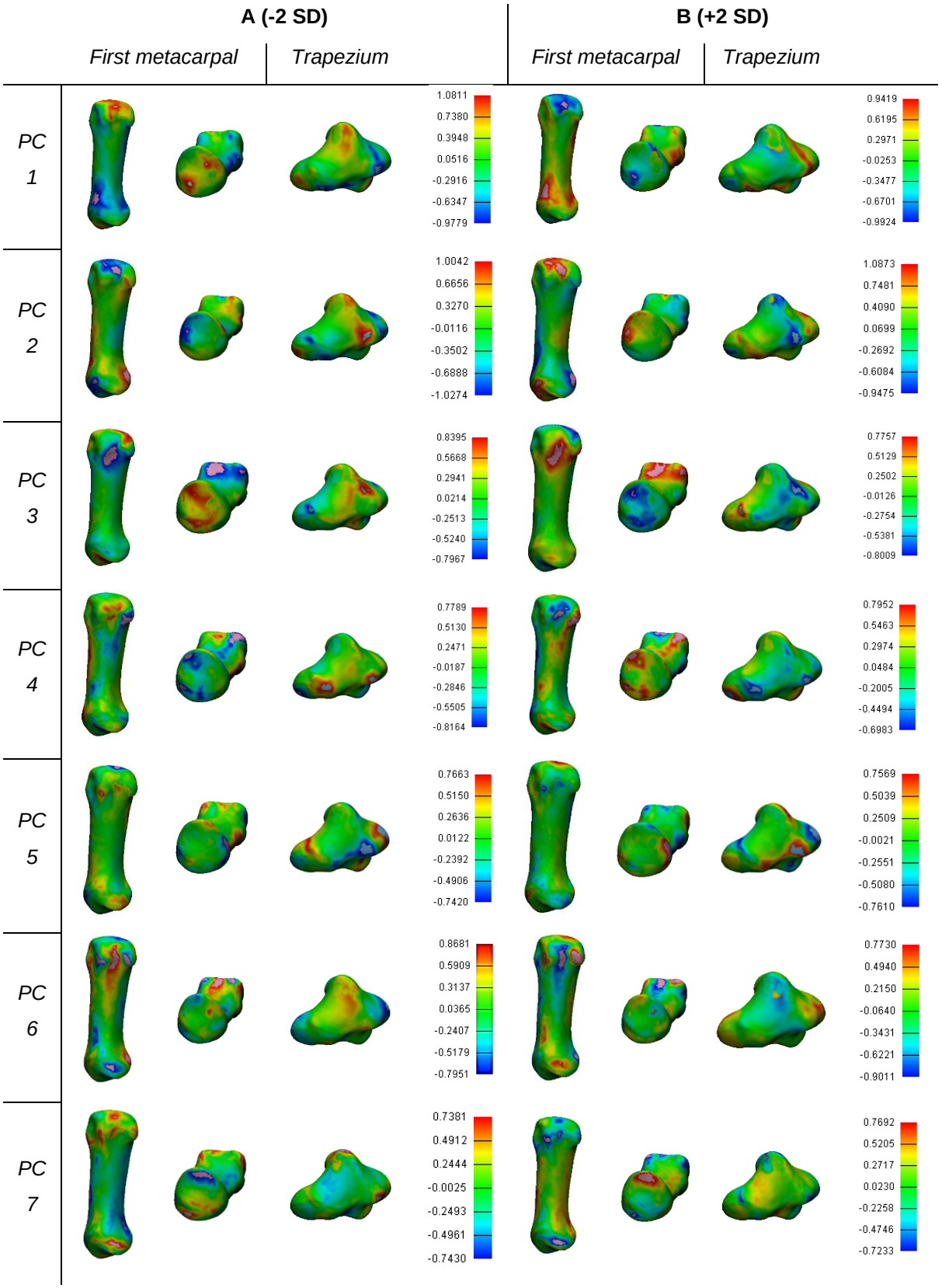

Figure 18 – Distances, in millimetres, between models for the first metacarpal and trapezium of the healthy T0 group, represented by seven PCs. The columns A exhibit the comparison between -2 SD and the mean model, while the columns B exhibit the comparison between +2 SD and the mean model. The colour grid represents the magnitude of the distances in millimetres.

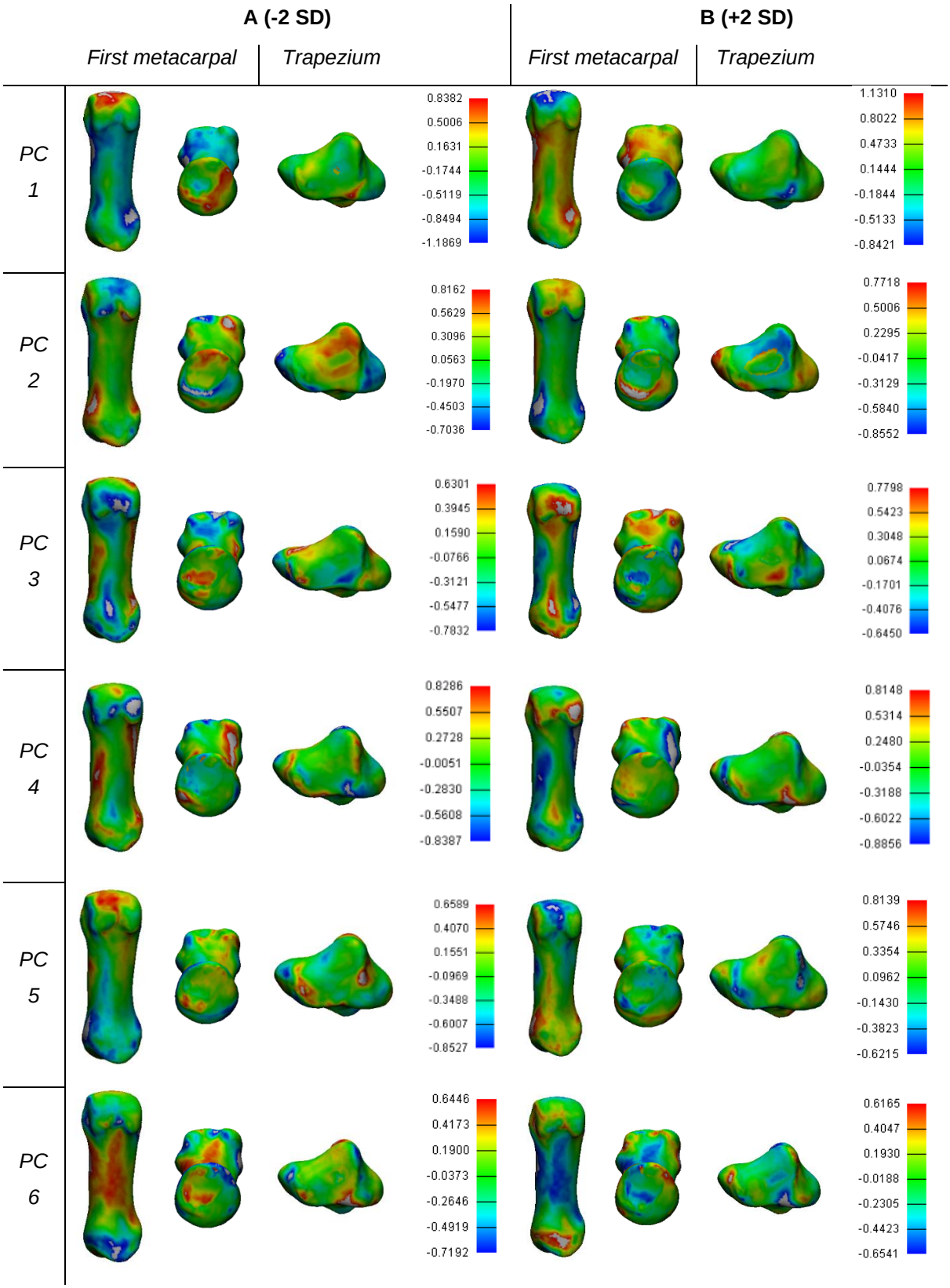

Figure 19 – Distances, in millimetres, between models for the first metacarpal and trapezium of the stabilised T0 group, represented by seven PCs. The columns A exhibit the comparison between -2 SD and the mean model, while the columns B exhibit the comparison between +2 SD and the mean model. The colour grid represents the magnitude of the distances in millimetres.

The distal and palmar sides, and the protuberances of the head exhibited, once again, variation in almost all PCs. Variations in the base were also found. All PCs presented variations on the volar beak, except the first and third PC that presented variation in the ulnar or the radial side. The articulating surface presented more variation in the palmar/radial ridge in the two first PCs, while the remaining PCs presented more variation in the palmar ridge.

- **Progressive**

The progressive population was diagnosed with stage I CMC-OA on T0 and stage II on T1. The four PC found relevant in this group are displayed in Figure 20. The first PC exhibited wider variation when compared not only to the remaining PCs of this population but also to those of the healthy and stabilised populations.

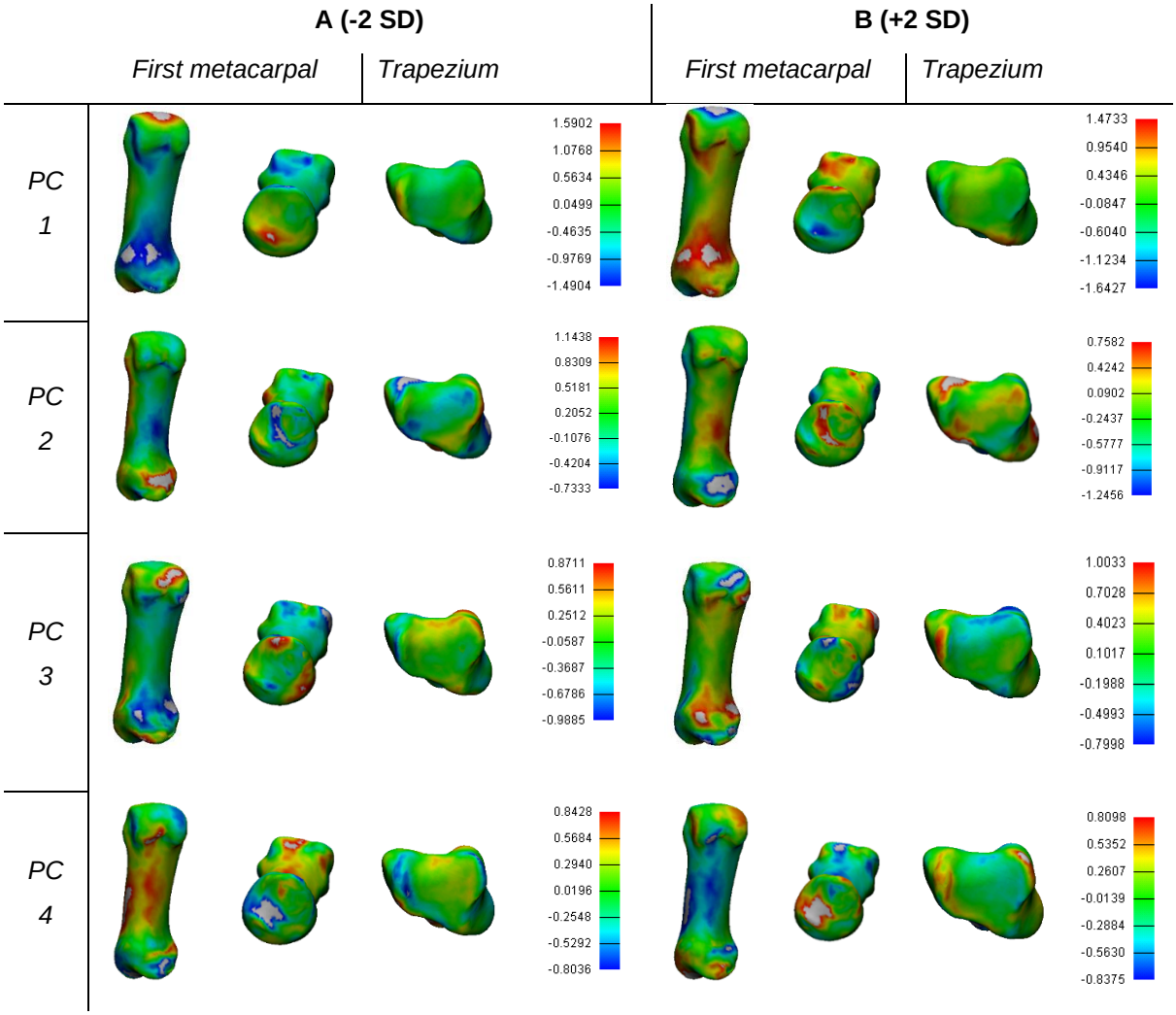

Figure 20 – Distances, in millimetres, between models for the first metacarpal and trapezium of the progressive T0 group, represented by seven PCs. The columns A exhibit the comparison between -2 SD and the mean model, while the columns B exhibit the comparison between +2 SD and the mean model. The colour grid represents the magnitude of the distances in millimetres.

The first metacarpal variations in this population were similar to those of the healthy and stable populations. The base of the first metacarpal presents strong variation, whether all around or in the distal side. The articulating surface exhibits more prominent variation in the palmar/ulnar ridge.

Regarding the trapezium, the variance was mostly observed on the periphery of the articulating surface and it was more concentrated. The first mode - that accounts for most of the cumulative variation - showed, generally, a small variation, which is more concentrated on the palmar depression and ulnar ridge.

4.2.2 Population comparison regarding time

The populations were characterized considering the T0 groups. In this subsection, the T0 and T1 groups of each population were compared to understand the differences in shape as a consequence of aging. This was achieved by comparing the mean model of each group within each population. Figure 21 presents the comparison between T0 and T1 groups of the healthy, stabilised and progressive populations. The variation range in shape, according to the colour grid, was wider in the progressive group (-1.0 mm to 1.1 mm) and narrower on the healthy group (-0.3 mm to 0.2 mm).

The healthy population, shown in Figure 21(a), exhibited more variation on the distal and palmar surfaces of the first metacarpal head. On the shaft there was small variance in the ulnar and radial region. The trapezium showed a noticeable peak of variation on the ulnar region. In the radial side, there is also variation, though less obvious.

The stabilised population, depicted in Figure 21(b), presented a little variation in the head, being more pronounced towards the radial region. On the shaft, there was variation in the ulnar region closer to the base of the first metacarpal. The trapezium presented more widespread variation. Looking to the articular surface, all peripheral regions presented notable variations. There was an increased variation in the ulnar side, but a slight decrease in the radial side. The palmar and dorsal sides presented small increases.

The progressive population, illustrated in Figure 21(c), was the one presenting the greatest variation. In the head of the first metacarpal at the distal side, there was no significant variation. However, in the palmar side, the left eminence exhibited negative variation and the ulnar and radial condyles exhibited differences as well. In the shaft, the variation was greater closer to the base of the first metacarpal bone, more prominent in the ulnar/palmar and radial regions. In the articulate surface, the ulnar/palmar region was more affected. In the trapezium articular surface, a marked variation was observed on the ulnar half. The remaining surface of the trapezium presented widespread variation.

Overall, the variations in the healthy population were not relevant when compared to the remaining populations. Moreover, comparing the variation sites between stabilised and progressive populations, it is noteworthy that the sites where the major variations occurred are similar. However, the intensity of the variations was stronger in the progressive population. In addition, the head of the first metacarpal also presented some variation in this population. At the base, besides ulnar variation, common to both stabilised and progressive populations, there was radial variation in the latter population.

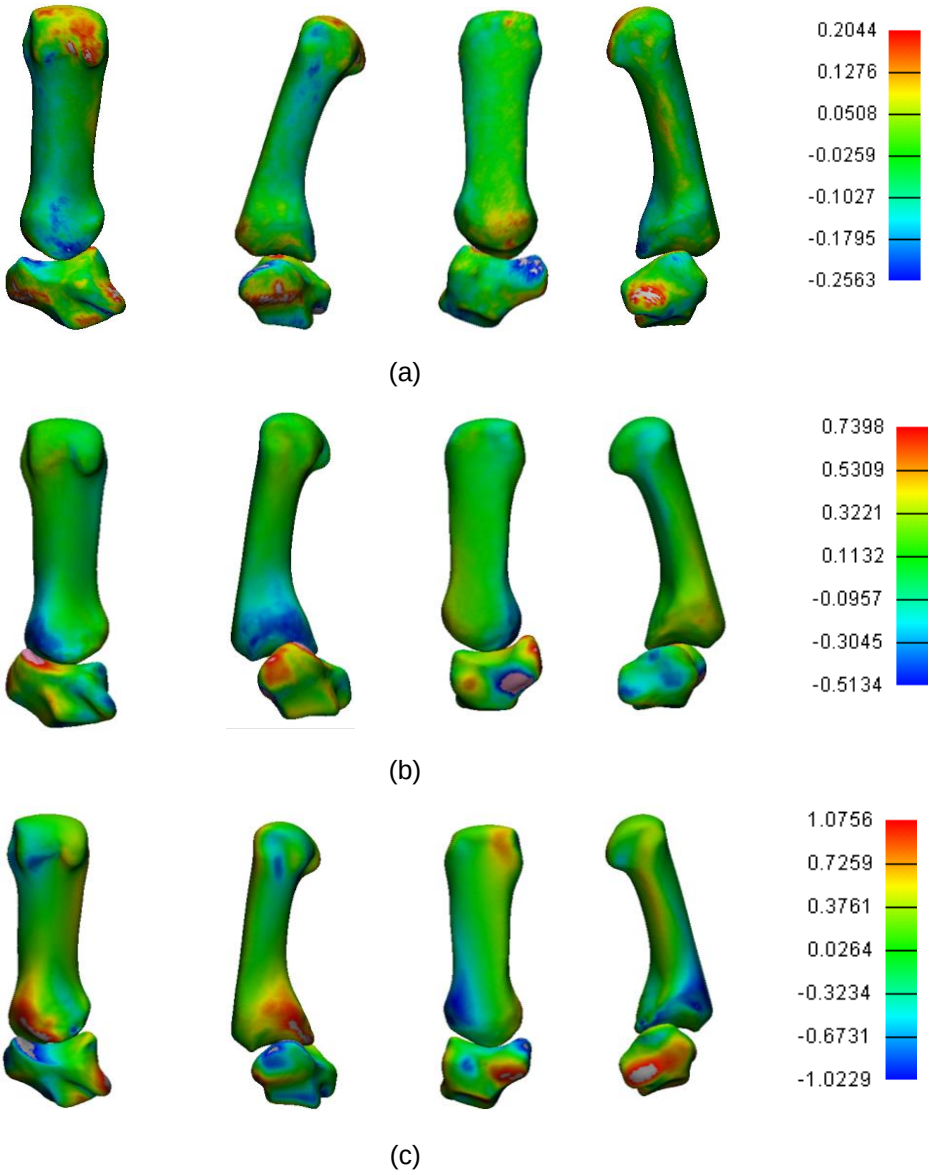

Figure 21 – Comparison between the initial and final time mean models for (a) the healthy, (b) stabilised, and (c) progressive populations. The colour grid represents the distances between models in millimetres.

4.2.3 Group comparison regarding condition

This analysis was meant to describe the differences regarding bone shape between different populations. Accordingly, comparisons between the healthy and the stabilised populations, as well as between groups presenting the same CMC-OA stage, were performed. Figure 22 illustrates the outcome of all comparisons performed.

The comparison between heathy and early stage OA, illustrated on Figure 22(a), showed a marked variation on the ulnar side of the volar beak of both the first metacarpal and the trapezium. The overlap of the two bone models, on the left, showed that for the early stage OA population, the bone suffered a

backwards translation, and a slight difference regarding bone length is visible. Besides that, the trapezium ulnar ridge was flat in the healthy population and more convex in stabilised population.

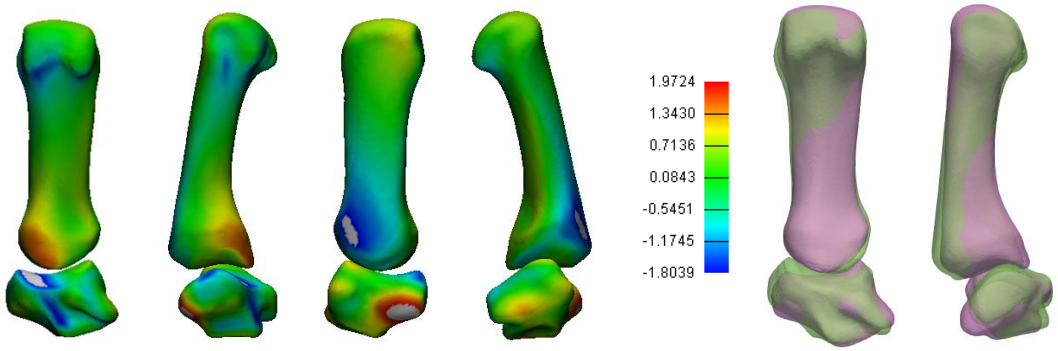

(a)

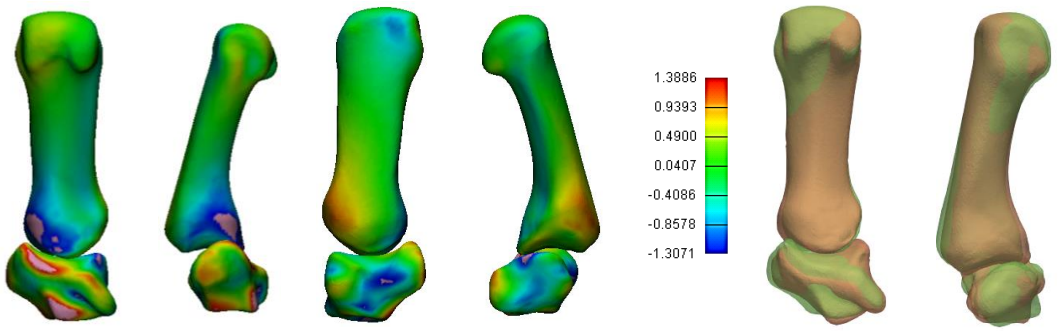

(b)

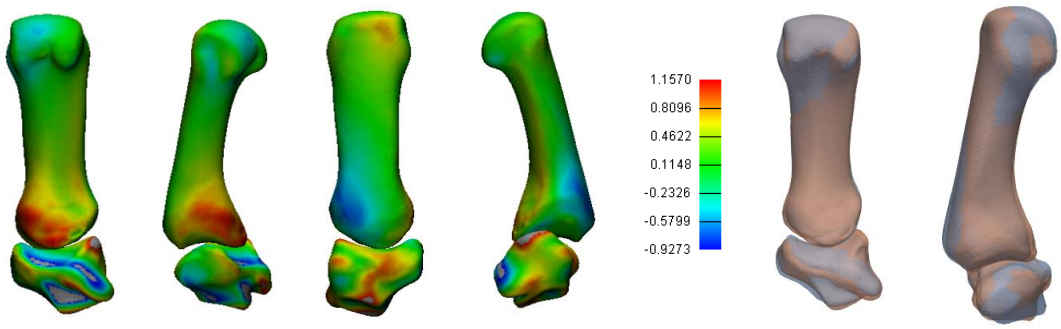

(c)

Figure 22 –Comparison between groups diagnosed with stage I OA at the first CMC joint: (a) Healthy T0 VS Stabilised T0, (b) Stabilised T0 VS Progressive T0, and (c) Progressive T0 VS Stabilised T1. The colour grid represents the distances between models in millimetres. Models on the left side are the overlap of the correspondent groups: purple-healthy T0, green-stabilised T0, orange-progressive T0, blue- stabilised T1.

From the comparison of the two populations that were diagnosed with stage I OA, i.e., stabilised T0 and progressive T0 groups, a negative variation at the volar beak in the ulnar region was identified at the base. In the radial region, a similar, but positive, variation was observed. Examining the trapezium, the variation was widely spread, and more visible along the radial ridge of the articulate surface.

The comparison between the progressive T0 group and stabilised T1 group showed a distribution of variations similar to that described for the stabilised and progressive T0 groups, although with less

variation. Both comparisons presented wider variation when compared to the analyses performed in Section 4.2.2. Although both groups were classified as having as stage I OA, there was significant variation between them. These comparisons could be interesting if the morphologic aspects that are linked with OA development are inherent to the individual and not an aspect that develops through time. More research needs to be employed in this topic.

4.3 Quantitative analysis

The measurement of morphologic parameters was the quantitative approach followed. As described in subsection 3.5.2, both bones of the first CMC joint were analysed. In the first metacarpal, the tilt and torsion angles were computed. In the trapezium, width and length were obtained. The present section displays the results and statistical analysis regarding these parameters.

In each group, the parameters were measured in the first two PCs. The variation of each PC was also included in this study. Therefore, in each group, the mean model, -2 SD, -1 SD, +1 SD and +2 SD models were assessed, and the morphologic parameters of these models were measured.

The morphologic parameters were measured for two PCs. Therefore, for each parameter, two measures exist (two PCs). In order to decide which PC better described each parameter, the Pearson correlation factor was assessed for the healthy, stabilised and progressive populations. The results can be found in Table 3, Table 4 and Table 5, respectively.

Observing Table 3, the tilt angle was the morphologic parameter that presented the highest correlations for both T0 and T1 groups, in both PCs. Even though all values were statistically significant, only one PC was selected for the following analysis. Therefore, the PC with the highest correlation was chosen. Analysing the values concerning the torsion angle, despite the fact that the correlation coefficient, at T0, not being strong or statistically significant, the second PC was chosen to represent this parameter since it presented the highest values. For the remaining parameters, concerning the trapezium, the same principles were applied. The only parameter that followed a strong linear distribution at both T0 and T1, was the tilt angle.

*Table 3 – Pearson correlation values, for the healthy population, between the morphologic parameters and weighing factor. *Correlation was statistically significant, p-value<0.05. Bold numbers indicate the chosen PC.*

	HEALTHY			
	T0		T1	
	PC1	PC2	PC1	PC2
Tilt	0.960*	**0.990***	**0.997***	0.955*
Torsion	0.537	**0.580**	**0.834**	0.632
Width	**0.883***	0.421	**0.713**	0.197
Length	0.387	**0.623**	**0.803**	0.984*

Considering the stabilised population, presented in the Table 4, the torsion angle was the parameter that best fitted a linear distribution, and thus higher correlation coefficients were obtained for it. The tilt angle in the T0 group also exhibited a strong linear distribution. The selection of PCs to consider for posterior analysis followed the same reasoning as that followed for the healthy population.

*Table 4 – Pearson correlation values, for the stabilised population, between the morphologic parameters and weighing factor. *Correlation was statistically significant, p-value<0.05. Bold numbers indicate the chosen PC.*

	STABILISED			
	T0		T1	
	PC1	PC2	PC1	PC2
Tilt	**0.979***	0.971*	**0.852**	0.563
Torsion	0.968*	**0.976***	0.410	**0.972***
Width	**0.702**	0.224	**0.832**	0.452
Length	0.868	**0.879***	0.202	**0.944***

Regarding the progressive population, both the tilt angle and width were parameters that fitted the linear distribution. The decisions concerning the cases for which there was no statistical significance, was made, as before, based on the highest correlation coefficient values.

*Table 5 – Pearson correlation values, for the progressive population, between the morphologic parameters and weighing factor. *Correlation was statistically significant, p-value<0.05. Bold numbers indicate the chosen PC.*

	PROGRESSIVE			
	T0		T1	
	PC1	PC2	PC1	PC2
Tilt	**0.941***	0.878	**0.976***	0.143
Torsion	0.646	**0.861**	**0.941***	0.540
Width	**0.934***	0.930*	0.031	**0.916***
Length	**0.880***	0.766	0.556	**0.996***

Having all the PCs chosen for the four parameters in each group, Table 6, Table 7 and Table 8 display the measurements that corresponded to the PC that best fitted the SD trend. For sake of briefness, the PC that presented measurements done are exhibited at Appendixes C.

From the analysis of Table 6 it was possible observe that in the tilt angle, that showed higher Pearson correlation coefficient, the values at T0 varied from -1.14 to 2.86 degrees, and from 4.48 to -3.51 degrees at T1. From the observation of the healthy population, the remaining parameters, torsion angle, width and length, the mean values did not vary much between T0 and T1.

Table 6 – Morphologic parameters measured for the healthy population. For the first metacarpal, tilt and torsion angles were measured in degrees, and for the trapezium, width and length were measured in milimetres.

HEALTHY								
Weighing factor	**T0**				T1			
	Tilt	*Torsion*	*Length*	*Width*	*Tilt*	*Torsion*	*Length*	*Width*
+2 SD	2.86	-23.93	9.88	13.65	4.48	6.37	9.80	15.23
+1 SD	1.97	16.32	9.58	13.36	2.55	3.19	10.16	14.25
mean	0.36	10.49	11.26	14.01	0.55	14.96	10.58	14.59
-1 SD	-0.27	15.30	10.81	14.24	-2.10	22.96	11.06	14.17
-2SD	-1.14	7.10	10.62	14.40	-3.51	18.14	11.14	14.29

Table 7 presents the measurements done for the stabilised population. The mean values of the first metacarpal parameters, between T0 and T1, have a two-degree difference. Concerning the trapezium, the mean values in both parameters and moments were quite similar. The ranges of the parameters did not vary much between moments, except for the tilt angle.

Table 7 – Morphologic parameters measured for the stabilised population. For the first metacarpal, tilt and torsion angles were measured in degrees, and for the trapezium, width and length were measured in milimetres.

STABILISED								
Weighing factor	**T0**				T1			
	Tilt	*Torsion*	*Length*	*Width*	*Tilt*	*Torsion*	*Length*	*Width*
+2 SD	7.26	7.26	10.13	13.43	5.14	6.37	9.14	12.68
+1 SD	6.74	12.31	10.16	12.88	4.86	3.19	9.61	13.19
mean	4.53	12.48	10.42	13.28	2.28	14.96	10.25	13.15
-1 SD	3.32	16.60	10.56	13.46	3.14	22.96	10.06	13.10
-2SD	0.04	18.17	11.60	14.22	2.27	18.14	10.81	13.48

Table 8 presents the measurements done in the progressive population. Observing the mean values of the four parameters between T0 and T1, it was possible to assess that while the tilt angle and length were similar, the torsion angle and width presented differences. Concerning the range of the parameters measured, there were more prominent change between T0 and T1.

Table 8 – Morphologic parameters measured for the progressive population. For the first metacarpal, tilt and torsion angles were measured in degrees, and for the trapezium, width and length were measured in milimetres.

PROGRESSIVE								
Weighing factor	**T0**				T1			
	Tilt	*Torsion*	*Length*	*Width*	*Tilt*	*Torsion*	*Length*	*Width*
+2 SD	12.16	9.37	12.90	18.81	-3.22	-3.59	15.00	19.56
+1 SD	8.95	6.32	13.30	17.90	1.02	8.11	14.31	18.80
mean	5.37	15.02	13.86	17.16	5.89	12.99	13.87	19.08
-1 SD	1.48	15.48	13.64	17.36	6.76	18.38	13.46	17.21
-2SD	-1.90	17.71	13.90	16.66	9.64	18.59	12.89	15.27

To assess if there were statistically significant differences between T0 and T1 in each population, a paired t-test was performed. This test was done with the parameters obtained. Before performing this test, the constraints that must be fulfilled for its application were verified, confirming its validity for the three populations.

As displayed in Table 9, the tilt angle, torsion angle, and width measurements did not exhibit statistically significant differences between T0 and T1 across all populations. Meaning that there were no differences between in these morphologic parameters between T0 and T1. The stabilised population presented a significant difference regarding the length of the trapezium articulating surface.

*Table 9 – P-values resulting from the paired t-test for the healthy, stabilised and progressive populations, between T0 and T1. *Statistically significant, p-value below 0.05.*

T0 VS T1	*Tilt*	*Torsion*	*Length*	*Width*
Healthy	0.408	0.358	0.637	0.143
Stabilised	0.565	0.105	0.012*	0.952
Progressive	0.981	0.550	0.511	0.506

With the aim of understanding if the parameters measured were significantly different between populations, and therefore able to distinguish OA condition, independent t-tests between populations were performed and charts displaying the mean and SD are presented. For each population, T0 groups were used for the comparisons. T0 groups were used because in the previous analysis all parameters, except trapezium's length on stabilised population, were considered changeless between T0 and T1.

The independent t-tests were performed comparing two populations at a time. The independent t-test has some constrains that needed to be verified previously. Apart from the torsion angle in the healthy T0 group, all measurements followed a normal distribution. For the healthy group, the torsion angle of the T1 group was used instead since it satisfied the normal distribution constraint.

Table 10 displays the p-values that resulted from the independent t-tests. Concerning the tilt angle, there were statistically significant differences between the healthy and stabilised populations, diagnosed with stage 0 and stage I OA, respectively. Between the healthy and progressive, and stabilised and progressive, populations the differences were not significant. Yet, the p-value between the healthy and progressive populations was closer to 0.05 than between the stabilised and progression populations. Regarding the torsion angle, no statistical significance was found. The p-values were close to 1. The comparison between the healthy and progressive, and stabilised and progressive, populations demonstrated to be statistically significant for the length. The comparison between healthy and stabilised populations revealed high p-values. Finally, considering the width, the progressive population was statistically significantly different from both stabilised and healthy populations, as found for the length. Although the healthy-stabilised comparison was not significantly different, its p-value was close to 0.05.

*Table 10 – P-value of the independent t-tests performed between populations for each morphological parameter. For first metacarpal, tilt and torsion angles were considered, and for the trapezium articulating surface, length and width were considered. *Statistically significant, p-value below 0.05.*

	Tilt	**Torsion**	**Length**	**Width**
Healthy - Stabilised	0.041*	0.955	0.734	0.138
Healthy - Progressive	0.128	0.937	0.000*	0.000*
Stabilised - Progressive	0.948	0.843	0.000*	0.000*

The charts presented in Figure 23 were developed to better visualise the results and interpret the statistical tests made, enabling also the visualisation of the range and amplitude of the parameters measured.

The tilt angle, displayed in Figure 23(a), shows a clear separation between healthy and stabilised populations, in agreement with the independent t-test. The progressive population mean was similar to that of the stabilised population. However, the progressive population presented wider tilt variation. The mean value of the tilt angle was lower for the healthy population (0.36º) than for the pathological population, including both stabilised (4.53º) and progressive (5.37º). Amongst populations, the mean torsion angles were similar between each other, but the variation values presented differences. In this parameter, the healthy group presented wider variation. Regarding length and width, there was a marked difference between the healthy and progressive populations. The population that accounted for more variation was the healthy population.

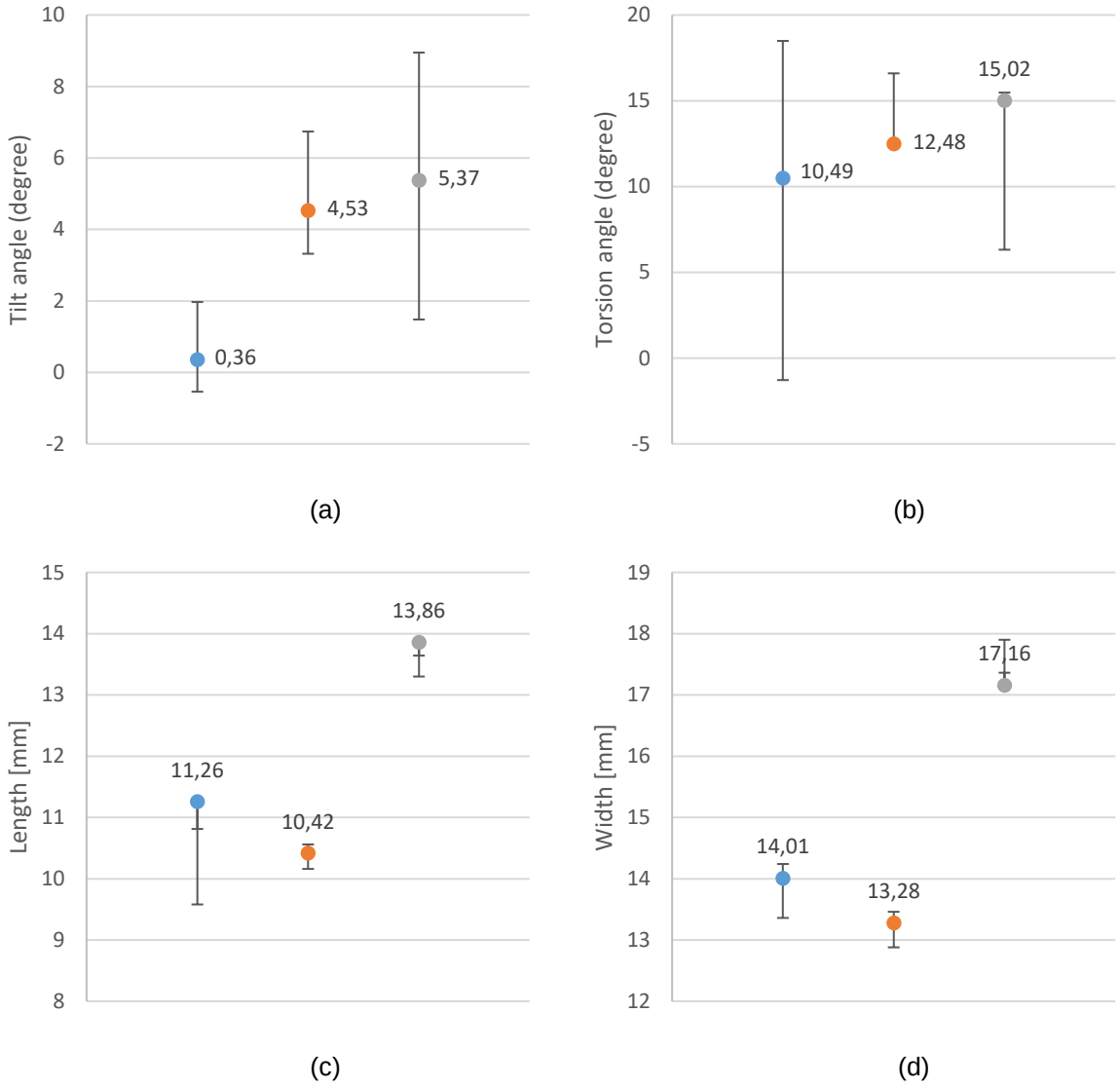

Figure 23 - Charts exhibiting mean value and -SD +SD of each population for: (a) tilt angle, (b) torsion angle, (c) length, and (d) width. The healthy, stabilised and progressive populations are denoted by blue, orange and grey markers, respectively.

5. DISCUSSION

In this section, the results are discussed and compared with the literature. For a better evaluation of the results, the methodology followed is also discussed.

5.1 Application of SSM

Statistical shape models have been widely used in the literature to assess bone shape and its variations (Tümer *et al.*, 2019; Schneider *et al.*, 2018; van de Giessen *et al.*, 2010; Chan *et al.*, 2013). Although its core goal is the same, its implementation could vary, and the results could vary with it. In the present work, the obtained results were generated through a recently developed SSM. The PCs resulted from an orthogonal transformation that aimed to arrange the dataset in such a way that the PCs were independent from one another. Each PC described a way in which that group could vary regarding bone shape. Since each group was run independently in SSM, there is no guarantee that the variation in the models corresponded among each other, which could have limited the analyses performed.

The variation of the first PC in the six groups evaluated varied between 10% and 14%. Although, usually, the first PC represents 50%-70% of total variation(Schneider *et al.*, 2018), Rusli & Kedgley (2019) and van de Giessen *et al.*, (2010) obtained similar variation in the first PC to the ones described. These low variation values are linked to the way SSM is implemented (Van De Giessen *et al.*, 2009), particularly due to the alignment and scaling of the different bone structures prior to the application of SSM. Nonetheless, these models have been proven to be representative in those researches (van de Giessen *et al.*, 2010). The SSM implementation used is state of the art, using multi-object SSM, where the morphological variations obtained from it do not neglect the morphological relationships between the first metacarpal and trapezium (Rusli & Kedgley, 2019). Besides that, the conducted study aimed at comparing populations, which has been weakly exploited in the literature.

Both groups of the healthy population, i.e., the T0 and T1 groups, presented the largest number of PCs with variance above 5%, even though they comprised less subjects. This could be linked with a more homogenous population. In the progressive population, where at T0 subjects were diagnosed with stage I OA and at T1 with stage II, the number of PCs that exhibited variance above 5% decreased. The cumulative variance they gathered decreased as well. This population presented a more heterogenous bone shape, which may be considered an indicative that bone shape varies depending on the health status of the subject. In fact, the most heterogenous population corresponded to the progressive population, and the more homogenous to the healthy population, which is consistent with the study of Kalichman & Hernández-Molina (2010).

5.2 Qualitative shape variation

The discussion regarding qualitative shape variation follows the order in which the results were presented.

Regarding the characterization of populations, some hypotheses can be formulated. In the stabilised and progressive populations, the variance in the shaft of the first metacarpal was more prominent than in the healthy population. These populations exhibited PCs with negative and positive variations in the ulnar and radial sides of the first metacarpal alternately. This could mean that one of the possible variations was a small rotation of the bone. Most of the PCs exhibited variation on the palmar ridge of the articulating surface of the first metacarpal, which could be linked with the length enlarging or even with rotation along the length of the bone. The trapezium articulating surface often exhibited variations on both ulnar and radial ridges. This could signify that there is a change in the articular surface concavity, which could influence the mobility of the first CMC joint and, ultimately, be linked with OA evolution. Although all three populations presented a broad variation, differences existed between them. Variations were stronger on the progressive population, and the variation distribution was different. The qualitative analysis of the differences in bone shapes, presented in Section 4.2.2, reinforces the hypothesis that a difference exists between the healthy and stabilised or progressive populations. Moreover, it provides the characterization of these populations for future work.

The comparison between T0 and T1 groups of the same population was performed to assess if aging plays an important factor regarding bone shape change. Again, the pathological population presented increasingly wider variation in comparison with the healthy population. Furthermore, even though the trapezium ulnar variation was observed in the three populations, the metacarpal sites where variation occurred changed completely between the healthy and pathological populations. Therefore, it could be suggested that the shape of the first CMC bones of a patient suffering from CMC-OA change over time in a different pattern than in a healthy person.

Finally, the three populations were compared directly. While comparing a healthy population with a population with early stage OA, Schneider *et al.* (2018) concluded that people who suffered from CMC-OA exhibited a lower aspect ratio (length to width ratio) exhibiting a shorter and thicker first metacarpal. The results obtained in the present work agree with these findings. In Section 4.2.3, the comparison between healthy and stabilised populations, that suffers from early stage OA, revealed that the first metacarpal of the healthy population was slightly longer and narrower than the first metacarpal of the stabilised population. Besides that, this comparison also brought to the attention that the stabilised population had the volar beak of the first metacarpal indented comparatively to the healthy population. This deterioration may be linked to the volar ligament degeneration that has been previously associated with OA (Doerschuk *et al.*, 1999; Pellegrini, 1991). In addition, Halilaj *et al.*, (2015a) reached the conclusion that the higher variation towards dorsovolar curvature of both metacarpal and trapezium, was linked to OA development. This is in agreement with the findings observed in this research, in the comparison between healthy and stabilised populations. Concerning the trapezium, the present work shows that while the healthy population exhibited the ulnar side of the articulating surface flat, the

stabilised population presented this ridge elevated, deepening the subchondral articular surface, this is displayed when directly comparing the healthy and progressive population at 4.2.3. These findings are similar to those reported by Schneider *et al.*, (2018) and Kovler *et al.*, (2004), which were not considered to cause OA development, but instead were associated with joint degeneration as a consequence.

In addition to this, through the comparison of stabilised and progressive population, the difference between populations for whom the disease progressed or not was also assessed. Although both groups compared were diagnosed with the same OA stage, the variation between them was relevant. However, it presented less variation than the previous comparison between two populations with different OA scores. There was major variation on the ulnar side of the volar beak, which could be linked, as stated before, with the volar ligament degeneration. The trapezium variations concentrated more on the periphery, and this behaviour was previously linked to osteophyte formation (Kovler *et al.*, 2004), which was expected since these populations suffer from OA.

The qualitative analyses performed suggest that there might exist differences among populations.

5.3 Morphologic parameters

The present research aimed to quantify morphologic parameters and correlate them with OA stage using multi-object SSM. Previous studies have tried to measure morphologic parameters in the first CMC joint, such as angles, in X-rays (Kurosawa, Tsuchiya & Takagishi, 2013). Yet, due to the incongruent configuration of the first CMC and to the 2D limitation of the X-ray, contributions to assess joint's stability have been limited. Research done with fluoroscopy, has dazed the 2D limitation, and made possible the assessment of morphologic parameters (Miura, Ohe & Masuko, 2004). Using this technique, volar tilt angle was studied amongst pathologic and control groups and found to be greater in pathological people. Despite the current study using CT data, this is consistent with the finding of Miura, Ohe & Masuko (2004). The tilt angle of the first metacarpal was found to be a statistically significant factor differentiating populations regarding their OA condition. The first metacarpal could be translated dorsally with high stress between the dorsal aspect of the articulating surfaces of the first metacarpal and trapezium (Kurosawa, Tsuchiya & Takagishi, 2013). This could explain why cartilage degradation is frequently observed to be initiated at the dorsal-radial region of the trapezium (Koff *et al.*, 2003). In this thesis, the same variation of the trapezium was found in the pathological population, further supporting this hypothesis. The torsion angle did not show specificity differentiating populations.

Concerning the trapezium articulating surface parameters, i.e., width and length. While on one hand they revealed to be significantly different between healthy and progressive populations, on the other hand, they showed differences between the stabilised and progressive groups, but no identifiable differences between the healthy and stabilised populations. The trapezium is a small bone that is under a lot of stress since its sides are all articulate surfaces of other joints, which can hamper its analysis and relations with CMC-OA. Besides that, by the analysis of the mean values for each population, it is possible to assess that pathological (progressive) people had greater length and width, which might

contribute for the degradation of joint's stability and allow wider movements that ultimately could disrupt other structures.

Regarding the comparison of the same population between T0 and T1, the morphologic parameters did not show significant differences. This goes in agreement with Chu *et al.*, (2012) that had previously stated that OA was a condition that takes decades to develop. In fact, in the present work, even when comparing progressive population between T0 and T1, there was no significant difference in bone morphology according to the parameters measured. If bone structure does not vary significantly over time, the parameters assessed could be suggested to be inherent over time. Thus, by their examination at any moment in time, the health status of the first CMC could be predicted. For this hypothesis to stand, the healthy and pathological populations should be significantly different from each other. As previously stated, the tilt angle revealed to be significantly different between the healthy and stabilised groups. However, no statistical significance was found between the healthy and progressive groups, even though the p-value was low.

Despite the analysis performed on the PCs relevant to be analysed, only the first two PCs were considered for the measurements of the morphological parameters discussed here. From the third PC on, measurements could not be performed due to the lack of definition in the bone shapes. Nonetheless, it is worth noting that the exclusion of all PCs apart from the first and second is expected to have little impact on the results since these two first PCs represented a significant share of variance.

6. CONCLUSIONS

The present work aimed to find if people with first CMC-OA and healthy people could be distinguished by assessing the morphology of their bones. To attain this goal a multi-object SSM was used in three populations, one healthy and two pathological. Followed by a qualitative and quantitative analysis, in which four morphological parameters were assessed, the tilt and torsion angle in the first metacarpal, and the length and width in the trapezium.

The results revealed that the tilt angle of the first metacarpal showed significant differences between healthy and early stage OA populations. This was the parameter, that together with the qualitative analysis, showed more robustness. No difference was detected when T0 and T1 were compared, demonstrating that aging did not influence bone morphology. The qualitative analysis also exhibited results supporting that it is possible to differentiate healthy and pathological populations through bone morphology. Pathological first metacarpals were narrower and thicker.

This study provided further insight into the morphological changes between healthy and CMC-OA populations, and suggested a novel morphological parameter that may be able to distinguish healthy from pathological people and possibly help predict OA. This would enable physicians to better diagnose and catch the disease in a less severe stage. The greater impact would be felt in the daily life of patients, whose life is impaired by this condition.

6.1 Limitations and future work

There are some limitations regarding the work developed that can be overcome in the future.

The scaphoid bone can also be analysed in future studies since in late stages of first CMC-OA this bone is highly affected. Including this bone in the study of shape could help understand the bone changes associated with this process.

The methodology followed for the measurements was mainly manual, which could lead to errors given the several points that had to be chosen and the variability in the data. An automated computed methodology would provide better consistency. Therefore, the development of an automated methodology is recommended to obtain more consistent measurements.

This work was performed using 3D models. However, the tools physicians have available to do screenings and standard diagnose is X ray, a 2D technique. Therefore, extended work must be done to translate the findings discovered to a 2D methodology assessed by X-ray.

In this work, SSM was applied to six different groups, which were afterwards compared given that each group was run individually, there was no way of guaranteeing that the variance in each PC corresponded among groups. To overcome this the Pearson correlation coefficient was employed. However, more research on this topic is required to find a robust way to compare populations that were analysed with the SSM used.

The study of bone morphology should be taken through a longer period as this can further unveil whether bone morphology is mutable or not.

7. REFERENCES

Arthritis Research UK (2013) Osteoarthritis in general practice - Data and Perspectives - Arthritis Research UK. *The Medical press*.222.

Badia, A. & Khanchandani, P. (2007) Thumb Carpometacarpal Joint Arthroscopy: A Classification System and Rationale for Treatment. *Operative Techniques in Orthopaedics*. [Online] 17 (2), 125–132. Available from: doi:10.1053/j.oto.2007.01.004.

Betts, J.G., Young, K.A., Wise, J.A., Johnson, E., et al. (2013) *Anatomy and Physiology*. Houston, Texas, OpenStax.

Brand, P.W. & Hollister, A. (1993) *Clinical Mechanics of the Hand*. Third edit. Michigan, Mosby.

Cardoso, F.N., Kim, H.J., Albertotti, F., Botte, M.J., et al. (2009) Imaging the ligaments of the trapeziometacarpal joint: MRI compared with MR arthrography in cadaveric specimens. *American Journal of Roentgenology*. [Online] 192 (1), 13–19. Available from: doi:10.2214/AJR.07.4010.

Chan, E.F., Farnsworth, C.L., Koziol, J.A., Hosalkar, H.S., et al. (2013) Statistical shape modeling of proximal femoral shape deformities in Legg-Calvé-Perthes disease and slipped capital femoral epiphysis. *Osteoarthritis and Cartilage*. [Online] 21 (3), 443–449. Available from: doi:10.1016/j.joca.2012.12.007.

Cho, H.J., Chang, C.B., Kim, K.W., Park, J.H., et al. (2011) Gender and Prevalence of Knee Osteoarthritis Types in Elderly Koreans. *Journal of Arthroplasty*. [Online] Available from: doi:10.1016/j.arth.2011.01.007.

Chu, C.R., Williams, A.A., Coyle, C.H. & Bowers, M.E. (2012) Early diagnosis to enable early treatment of pre-osteoarthritis. *Arthritis Research and Therapy*. [Online] 14 (3). Available from: doi:10.1186/ar3845.

Cootes, T., Taylor, C., Cooper & J., G. (1995) Active Shape Models - Their Training and Application. *Computer Vision and Image Understanding*. 61 (1), 38–59.

Croux, C., Filzmoser, P. & Oliveira, M.R. (2007) Algorithms for Projection-Pursuit robust principal component analysis. *Chemometrics and Intelligent Laboratory Systems*. [Online] 87 (2), 218–225. Available from: doi:10.1016/j.chemolab.2007.01.004.

Crum, W.R., Hartkens, T. & Hill, D.L.G. (2004) Non-rigid image registration: Theory and practice. *British Journal of Radiology*. [Online] 77, 140–153. Available from: doi:10.1259/bjr/25329214.

Doerschuk, S.H., Hicks, D.G., Chinchilli, V.M. & Pellegrini, V.D. (1999) Histopathology of the palmar beak ligament in trapeziometacarpal osteoarthritis. *Journal of Hand Surgery*. [Online] 24 (3), 496–504. Available from: doi:10.1053/jhsu.1999.0496.

Eaton, R.G., Lane, L.B., Littler, J.W. & Keyser, J.J. (1984) Ligament reconstruction for the painful thumb

carpometacarpal joint: A long-term assessment. *Journal of Hand Surgery*. [Online] 9 (5), 692–699. Available from: doi:10.1016/S0363-5023(84)80015-5.

Egan, M.Y. & Brousseau, L. (2007) Splinting for osteoarthritis of the carpometacarpal joint: A review of the evidence. *American Journal of Occupational Therapy*. [Online] 61 (1), 70–78. Available from: doi:10.5014/ajot.61.1.70.

Fitzgibbon, A.W. (2003) Robust registration of 2D and 3D point sets. *Image and Vision Computing*. [Online] 21 (13–14), 1145–1153. Available from: doi:10.1016/j.imavis.2003.09.004.

van de Giessen, M., Foumani, M., Streekstra, G.J., Strackee, S.D., et al. (2010) Statistical descriptions of scaphoid and lunate bone shapes. *Journal of Biomechanics*. [Online] 43 (8), 1463–1469. Available from: doi:10.1016/j.jbiomech.2010.02.006.

Van De Giessen, M., Streekstra, G.J., Strackee, S.D., Maas, M., et al. (2009) Constrained registration of the wrist joint. *IEEE Transactions on Medical Imaging*. [Online] 28 (12), 1861–1869. Available from: doi:10.1109/TMI.2009.2021432.

Gillis, J., Calder, K. & Williams, J. (2011) Review of thumb carpometacarpal arthritis classification, treatment and outcomes. *Canadian Journal of Plastic Surgery*. [Online] 19 (4), 134–138. Available from: doi:10.1177/229255031101900409.

Gray, H. & Lewis, W.H. (1918) *Gray's Anatomy of the Human Body*. 20th edition. Lea & Febiger (ed.). Philadelphia, PA.

Gregory, J.S., Waarsing, J.H., Day, J., Pols, H.A., et al. (2007) Early identification of radiographic osteoarthritis of the hip using an active shape model to quantify changes in bone morphometric features: Can hip shape tell us anything about the progression of osteoarthritis? *Arthritis and Rheumatism*. [Online] 56 (11), 3634–3643. Available from: doi:10.1002/art.22982.

Groth, D., Hartmann, S., Klie, S. & Selbig, J. (2013) Principal components analysis. *Methods in Molecular Biology*. [Online] 930, 527–547. Available from: doi:10.1007/978-1-62703-059-5_22.

Halilaj, E., Moore, D.C., Laidlaw, D.H., Got, C.J., et al. (2014) The morphology of the thumb carpometacarpal joint does not differ between men and women, but changes with aging and early osteoarthritis. *Journal of Biomechanics*. [Online] 47 (11), 2709–2714. Available from: doi:10.1016/j.jbiomech.2014.05.005.

Halilaj, E., Moore, D.C., Patel, T.K., Ladd, A.L., et al. (2015a) Early osteoarthritis of the trapeziometacarpal joint is not associated with joint instability during typical isometric loading. *Journal of Orthopaedic Research*. [Online] 33 (11), 1639–1645. Available from: doi:10.1002/jor.22936.

Halilaj, E., Moore, D.C., Patel, T.K., Laidlaw, D.H., et al. (2015b) Older asymptomatic women exhibit patterns of thumb carpometacarpal joint space narrowing that precede changes associated with early osteoarthritis. *Journal of Biomechanics*. [Online] 48 (13), 3634–3640. Available from: doi:10.1016/j.jbiomech.2015.08.010.

Hernández-Díaz, C., Van-Schoor, N. & Aboul Fotouh Khalil, A. (2017) Hand Osteoarthritis: An Epidemiological Perspective. *Comorbidity in Rheumatic Diseases*. [Online] 58, 197–206. Available from: doi:10.1007/978-3-319-59963-2_9.

Hunter, D.J. & Bierma-Zeinstra, S. (2006) Osteoarthritis. *The Lancet*. [Online] 58, 150–167. Available from: doi:10.1016/S0140-6736(19)30417-9.

Kalichman, L. & Hernández-Molina, G. (2010) Hand osteoarthritis: An epidemiological perspective. *Seminars in Arthritis and Rheumatism*. [Online] 39 (6), 465–476. Available from: doi:10.1016/j.semarthrit.2009.03.001.

Kennedy, C.D., Manske, M.C. & Huang, J.I. (2016) Classifications in Brief: The Eaton-Littler Classification of Thumb Carpometacarpal Joint Arthrosis. *Clinical Orthopaedics and Related Research*. [Online] 474 (12), 2729–2733. Available from: doi:10.1007/s11999-016-4864-6.

Koff, M.F., Ugwonali, O.F., Strauch, R.J., Rosenwasser, M.P., et al. (2003) Sequential wear patterns of the articular cartilage of the thumb carpometacarpal joint in osteoarthritis. *Journal of Hand Surgery*. [Online] 28 (4), 597–604. Available from: doi:10.1016/S0363-5023(03)00145-X.

Kovler, M., Lundon, K., McKee, N. & Agur, A. (2004) The human first carpometacarpal joint: Osteoarthritic degeneration and 3-dimensional modeling. *Journal of Hand Therapy*. [Online] 17 (4), 393–400. Available from: doi:10.1197/j.jht.2004.07.001.

Kubik, N.J. & Lubahn, J.D. (2002) Intrarater and interrater reliability of the Eaton classification of basal joint arthritis. *Journal of Hand Surgery*. [Online] 27 (5), 882–885. Available from: doi:10.1053/jhsu.2002.35310.

Kurosawa, K., Tsuchiya, I. & Takagishi, K. (2013) Trapezial-metacarpal joint arthritis: Radiographic correlation between first metacarpal articular tilt and dorsal subluxation. *Journal of Hand Surgery*. [Online] 38 (2), 302–308. Available from: doi:10.1016/j.jhsa.2012.09.027.

Ladd, A., MD, A.-P., Weiss, C., MD, J., et al. (2013a) The Thumb Carpometacarpal Joint: Anatomy, Hormones, and Biomechanics. *Bone*. [Online] 62 (1), 165–179. Available from: doi:10.1038/jid.2014.371.

Ladd, A.L., Weiss, A.-P.C., Crisco, J.J., Hagert, E., et al. (2013b) The thumb carpometacarpal joint: anatomy, hormones, and biomechanics. *Instructional course lectures*. [Online] 62, 165–179. Available from: http://www.ncbi.nlm.nih.gov/pubmed/23395023%0Ahttp://www.pubmedcentral.nih.gov/articlerender.fcgi?artid=PMC3935621.

Lara, V.S., Consolaro, A. & Bruce, R.S. (2000) Macroscopic and microscopic analysis of the palato-gingival groove. *Journal of Endodontics*. [Online] 26 (6), 345–350. Available from: doi:10.1097/00004770-200006000-00009.

Li, Q., Amano, K., Link, T.M. & Ma, C.B. (2016) Advanced Imaging in Osteoarthritis. *Sports Health*. [Online] 8 (5), 418–428. Available from: doi:10.1177/1941738116663922.

Liu, Y., Dong, X. & Peng, W. (2010) Study on digital data processing techniques for 3D medical model. *2010 4th International Conference on Bioinformatics and Biomedical Engineering, iCBBE 2010*. [Online] 2–5. Available from: doi:10.1109/ICBBE.2010.5518168.

Melville, D.M., Taljanovic, M.S., Scalcione, L.R., Eble, J.M., et al. (2015) Imaging and management of thumb carpometacarpal joint osteoarthritis. *Skeletal Radiology*. [Online] 44 (2), 165–177. Available from: doi:10.1007/s00256-014-1997-0.

Menon, J. (1996) Arthroscopic management of trapeziometacarpal joint arthritic of the thumb. *Arthroscopy*. [Online] 12 (5), 581–587. Available from: doi:10.1016/S0749-8063(96)90198-X.

Miura, T., Ohe, T. & Masuko, T. (2004) Comparative in Vivo Kinematic Analysis of Normal and Osteoarthritic Trapeziometacarpal Joints. *Journal of Hand Surgery*. [Online] 29 (2), 252–257. Available from: doi:10.1016/j.jhsa.2003.11.002.

Myronenko, A. & Song, X. (2010) Point set registration: Coherent point drifts. *IEEE Transactions on Pattern Analysis and Machine Intelligence*. [Online] 32 (12), 2262–2275. Available from: doi:10.1109/TPAMI.2010.46.

Neogi, T., Bowes, M.A., Niu, J., De Souza, K.M., et al. (2013) Magnetic resonance imaging-based three-dimensional bone shape of the knee predicts onset of knee osteoarthritis: Data from the osteoarthritis initiative. *Arthritis and Rheumatism*. [Online] 65 (8), 2048–2058. Available from: doi:10.1002/art.37987.

Neumann, D.A. & Bielefeld, T. (2003) The Carpometacarpal Joint of the Thumb: Stability, Deformity, and Therapeutic Intervention. *Journal of Orthopaedic & Sports Physical Therapy*. 33 (7), 386–399.

Patel, T.J., Beredjiklian, P.K. & Matzon, J.L. (2013) Trapeziometacarpal joint arthritis. *Current Reviews in Musculoskeletal Medicine*. [Online] 6 (1), 1–8. Available from: doi:10.1007/s12178-012-9147-6.

Pellegrini, V.D. (1991) Osteoarthritis of the trapeziometacarpal joint: The pathophysiology of articular cartilage degeneration. I. Anatomy and pathology of the aging joint. *Journal of Hand Surgery*. [Online] 16 (6), 967–974. Available from: doi:10.1016/S0363-5023(10)80054-1.

Riancho, J.A., García-Ibarbia, C., Gravani, A., Raine, E.V.A., et al. (2010) Common variations in estrogen-related genes are associated with severe large-joint osteoarthritis: A multicenter genetic and functional study. *Osteoarthritis and Cartilage*. [Online] Available from: doi:10.1016/j.joca.2010.04.002.

Rodolà, E., Albarelli, A., Cremers, D. & Torsello, A. (2015) A simple and effective relevance-based point sampling for 3D shapes. *Pattern Recognition Letters*. [Online] 59, 41–47. Available from: doi:10.1016/j.patrec.2015.03.009.

Dela Rosa, T.L., Vance, M.C. & Stern, P.J. (2004) Radiographic Optimization of the Eaton Classification. *Hand Surgery*. 29 (2), 173–177.

Ross, S.M. (2012) *Introduction to Probability and Statistics for Engineers and Scientists*. Third. [Online]. Available from: doi:10.1017/CBO9781107415324.004.

Rusli, W.M.R. & Kedgley, A.E. (2019) *Statistical shape modelling of the first carpometacarpal joint reveals high variation in morphology*. Unpubished.

Schieber, M.H. & Santello, M. (2004) Hand function: Peripheral and central constraints on performance. *Journal of Applied Physiology*. [Online] 96 (6), 2293–2300. Available from: doi:10.1152/japplphysiol.01063.2003.

Schneider, M.T.Y., Zhang, J., Walker, C.G., Crisco, J.J., et al. (2018) Early morphologic changes in trapeziometacarpal joint bones with osteoarthritis. *Osteoarthritis and Cartilage*. [Online] 26 (10), 1338–1344. Available from: doi:10.1016/j.joca.2018.06.008.

Schreiber, J.J., McQuillan, T.J., Halilaj, E., Crisco, J.J., et al. (2018) Changes in Local Bone Density in

Early Thumb Carpometacarpal Joint Osteoarthritis. *Journal of Hand Surgery*. [Online] 43 (1), 33–38. Available from: doi:10.1016/j.jhsa.2017.09.004.

Sharma, N. & Aggarwal, L.M. (2010) Automated medical image segmentation technique. *Journal of Medical Physics*. 35 (1), 3–14.

Tortora, G.J. & Derrickson, B. (2014) *The digestive system and homeostasis.Principles of Anatomy & Physiology*. 14th edition.

Tümer, N., Arbabi, V., Gielis, W.P., de Jong, P.A., et al. (2019) Three-dimensional analysis of shape variations and symmetry of the fibula, tibia, calcaneus and talus. *Journal of Anatomy*. [Online] 234 (1), 132–144. Available from: doi:10.1111/joa.12900.

Waldman, S.D. (2009) *The Carpometacarpal Joints of the Fingers*. Steven D. Waldman (ed.). [Online]. Saunders. Available from: doi:10.1016/b978-1-4160-5893-9.00056-3.

Weiss, E. & Jurmain, R. (2007) Osteoarthritis Revisited: A Contemporary Review of Aetiology. *International Journal of Osteoarchaeology*. [Online] 234 (April 2006), 437–450. Available from: doi:10.1002/oa.

Wu, G., Van Der Helm, F.C.T., Veeger, H.E.J., Makhsous, M., et al. (2005) ISB recommendation on definitions of joint coordinate systems of various joints for the reporting of human joint motion - Part II: Shoulder, elbow, wrist and hand. *Journal of Biomechanics*. [Online] 38 (5), 981–992. Available from: doi:10.1016/j.jbiomech.2004.05.042.

APPENDIXES

This section is divided into three parts. Subsection A contains the charts that show the variance and cumulative variance of the PCs after SSM. They correspond to the remaining groups that were not displayed in Section 4.1. Subsection B comprises the relevant PCs of T1 groups of healthy stabilised and progressive populations that were not displayed in section 4.2.1. Finally, subsection C comprises the measurements of the first and second PC for the four morphologic parameters for each group and population.

A

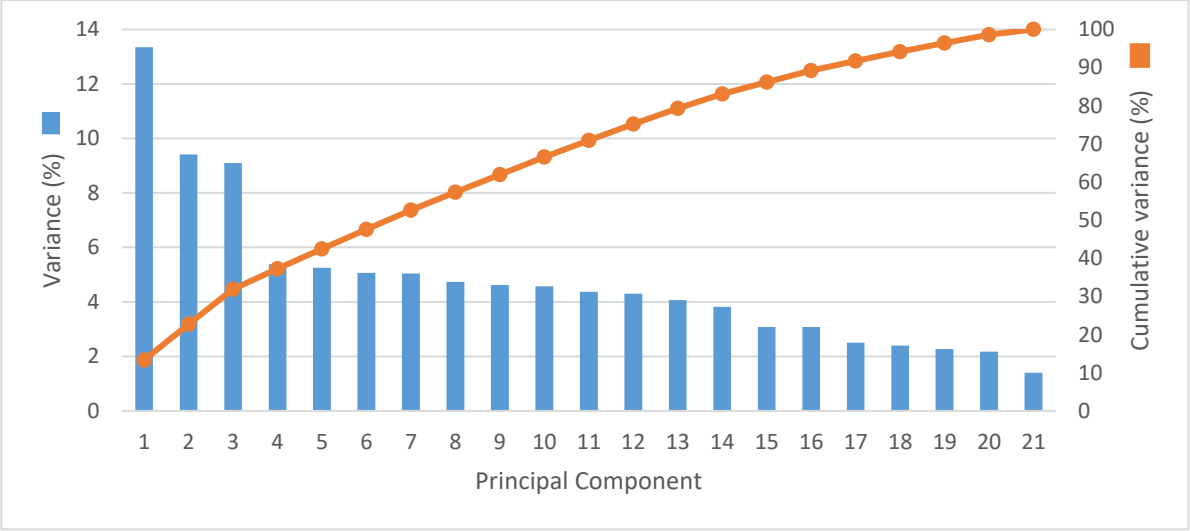

Figure 24 – Variance and cumulative variance of the healthy group at T0 explained by 21 PCs of the SSM.

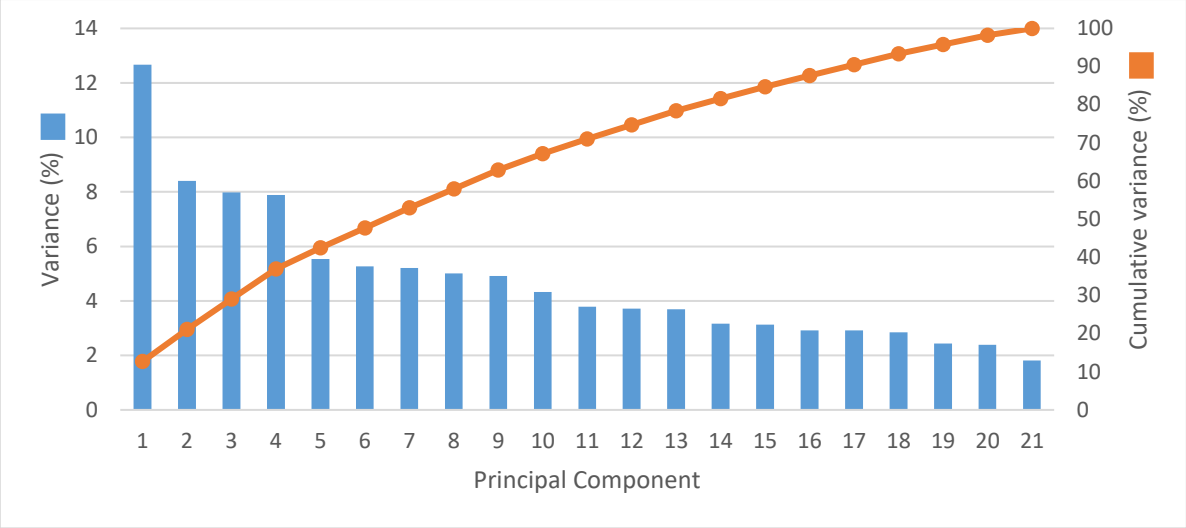

Figure 25 – Variance and cumulative variance of the healthy group at T1 explained by 21 PCs of the SSM.

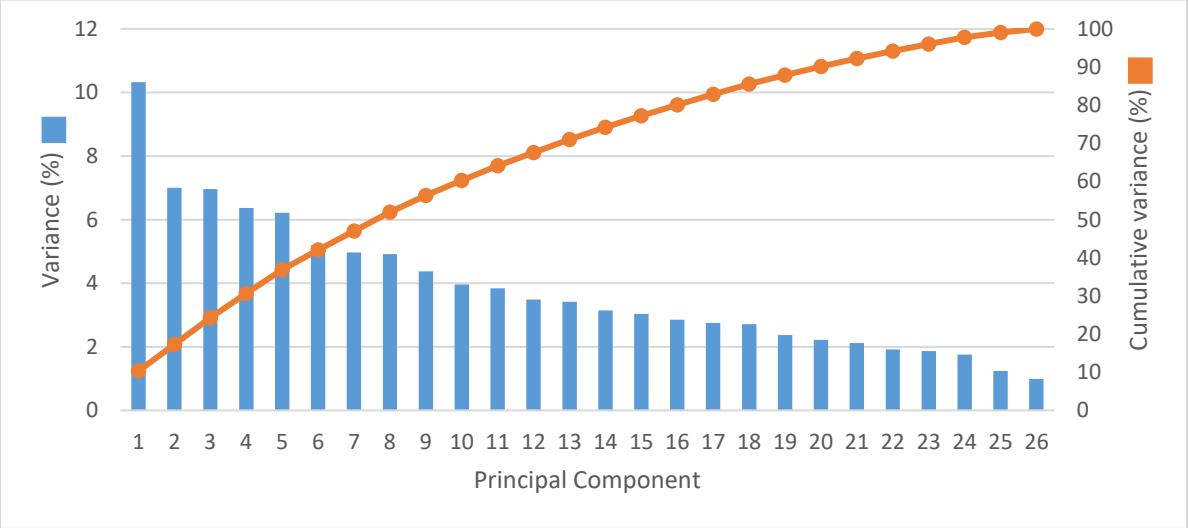

Figure 26 – Variance and cumulative variance of the stabilised group at T0 explained by 26 PCs of the SSM.

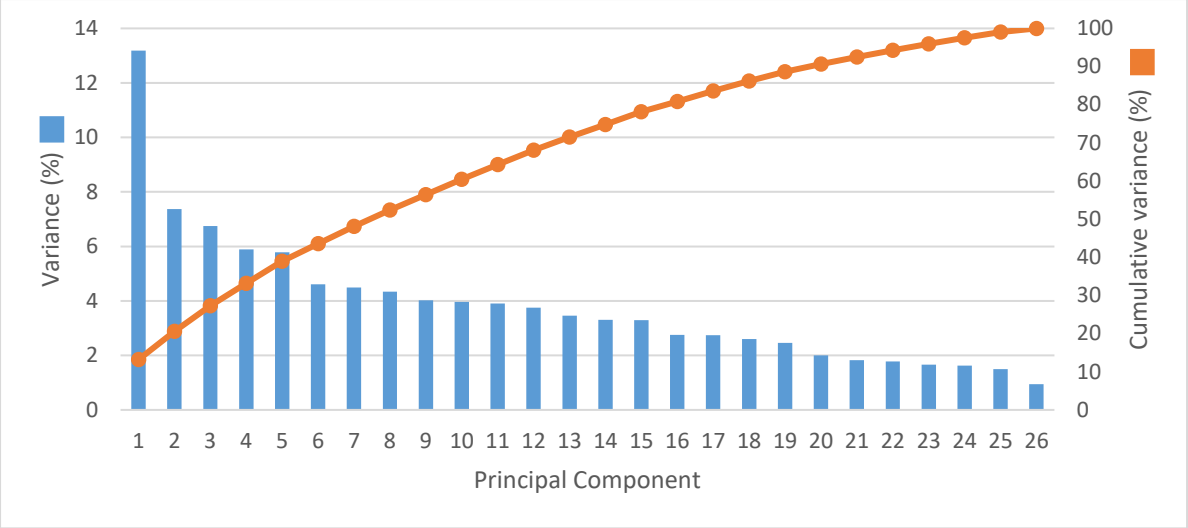

Figure 27 – Variance and cumulative variance of the stabilised group at T1 explained by 26 PCs of the SSM.

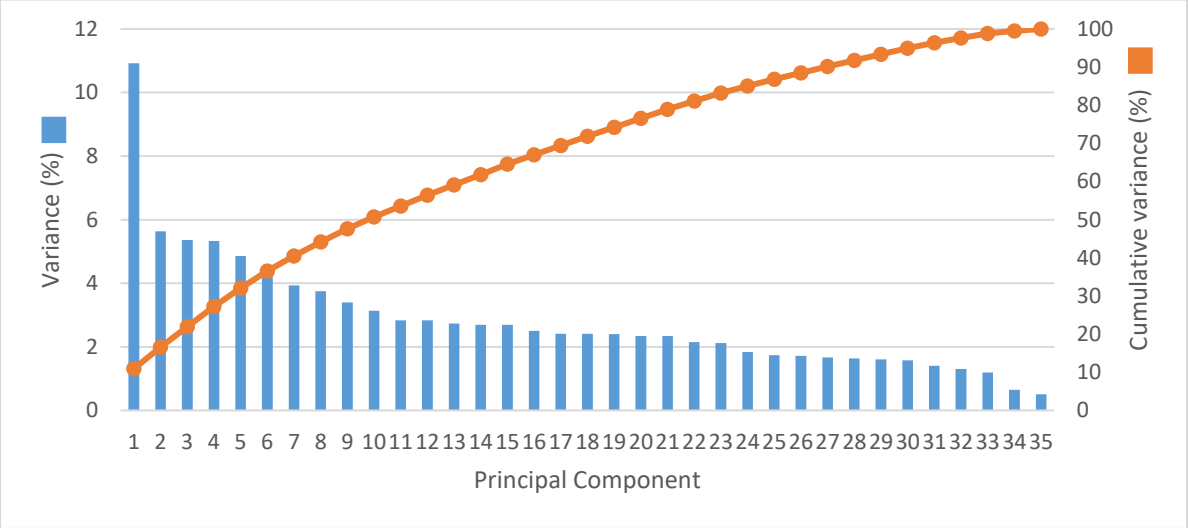

Figure 28 – Variance and cumulative variance of the progressive group at T1 explained by 35 PCs of the SSM.

B

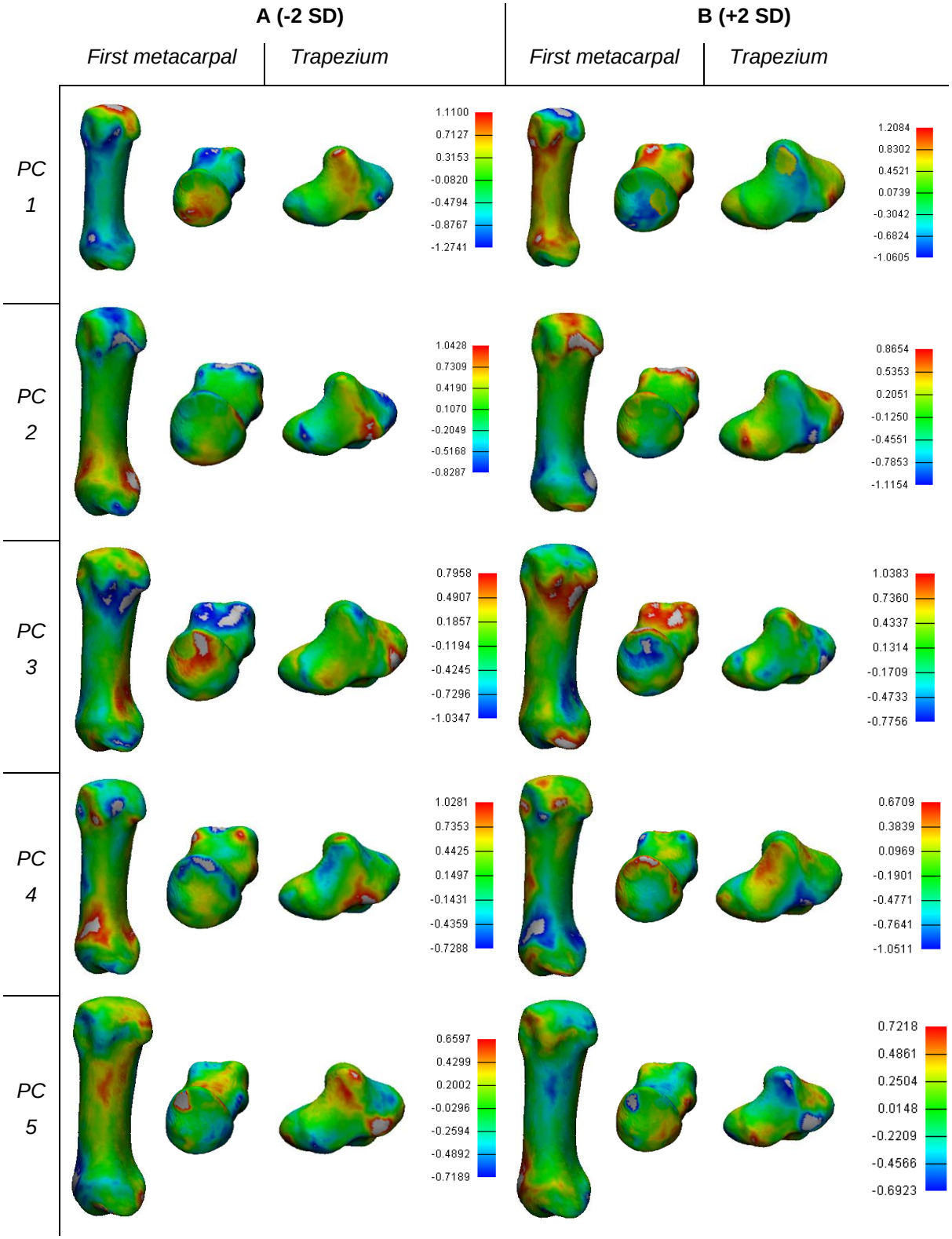
A (-2 SD)
B (+2 SD)
First metacarpal
Trapezium
First metacarpal
Trapezium
PC 1
1.1100
0.7127
0.3153
-0.0820
-0.4794
-0.8767
-1.2741
1.2084
0.8302
0.4521
0.0739
-0.3042
-0.6824
-1.0605
PC 2
1.0428
0.7309
0.4190
0.1070
-0.2049
-0.5168
-0.8287
0.8654
0.5353
0.2051
-0.1250
-0.4551
-0.7853
-1.1154
PC 3
0.7958
0.4907
0.1857
-0.1194
-0.4245
-0.7296
-1.0347
1.0383
0.7360
0.4337
0.1314
-0.1709
-0.4733
-0.7756
PC 4
1.0281
0.7353
0.4425
0.1497
-0.1431
-0.4359
-0.7288
0.6709
0.3839
0.0969
-0.1901
-0.4771
-0.7641
-1.0511
PC 5
0.6597
0.4299
0.2002
-0.0296
-0.2594
-0.4892
-0.7189
0.7218
0.4861
0.2504
0.0148
-0.2209
-0.4566
-0.6923

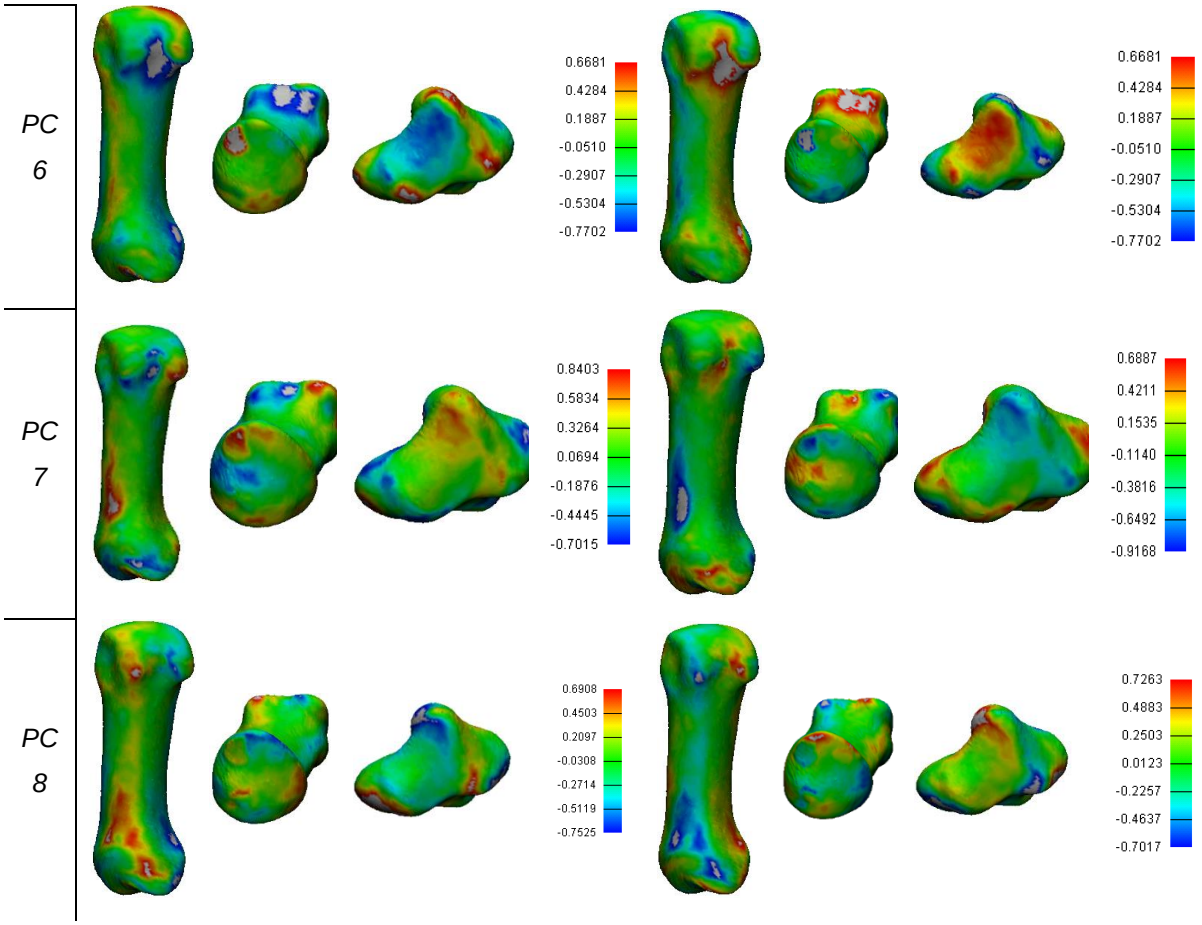

Figure 29 – Distances, in millimetres, between models for the first metacarpal and trapezium of the healthy T1 group, represented by seven PCs. The columns A exhibit the comparison between -2 SD and the mean model, while the columns B exhibit the comparison between +2 SD and the mean model. The colour grid represents the magnitude of the distances.

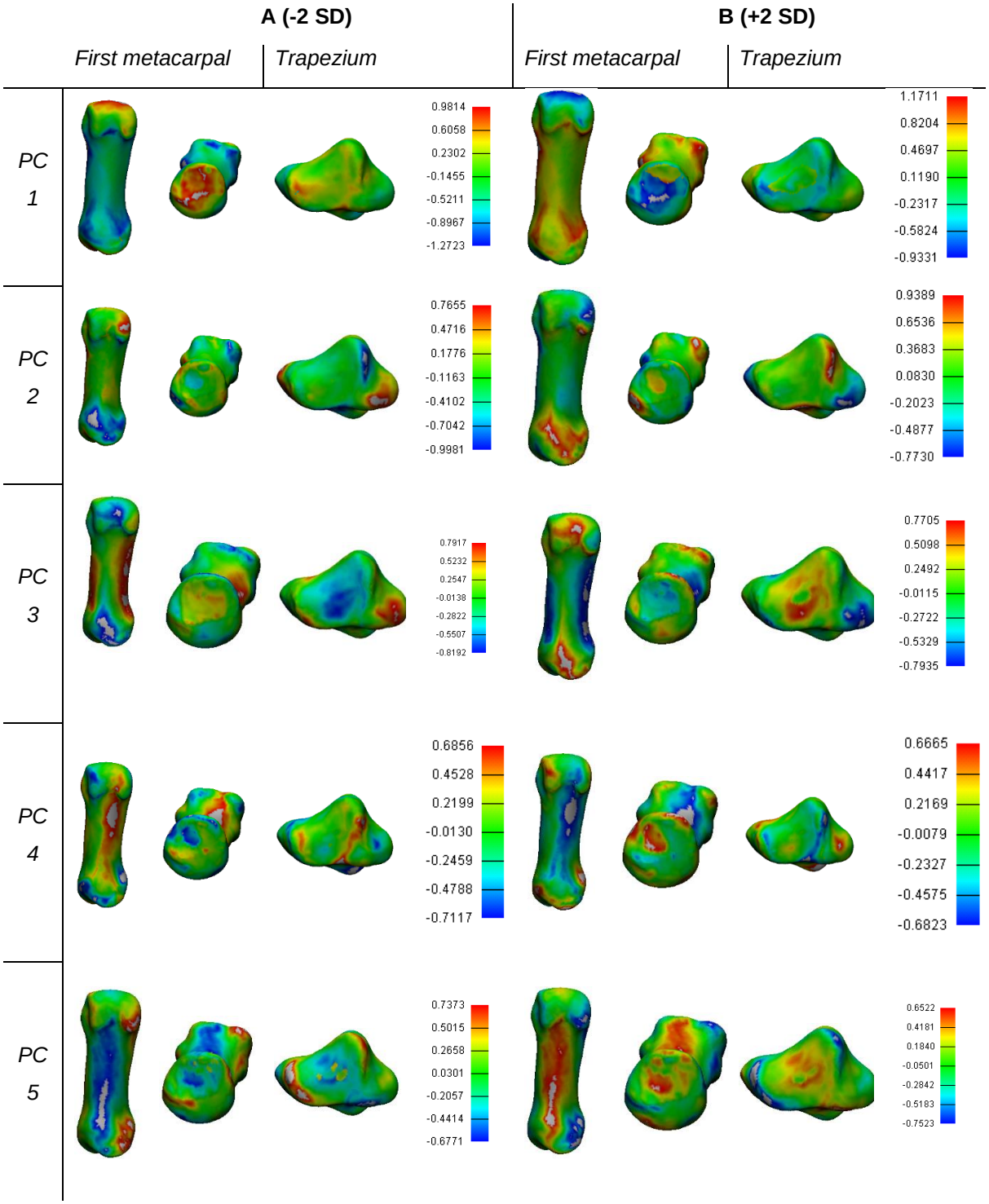

Figure 30 – Distances, in millimetres, between models for the first metacarpal and trapezium of the stabilised T1 group, represented by seven PCs. The columns A exhibit the comparison between -2 SD and the mean model, while the columns B exhibit the comparison between +2 SD and the mean model. The colour grid represents the magnitude of the distances.

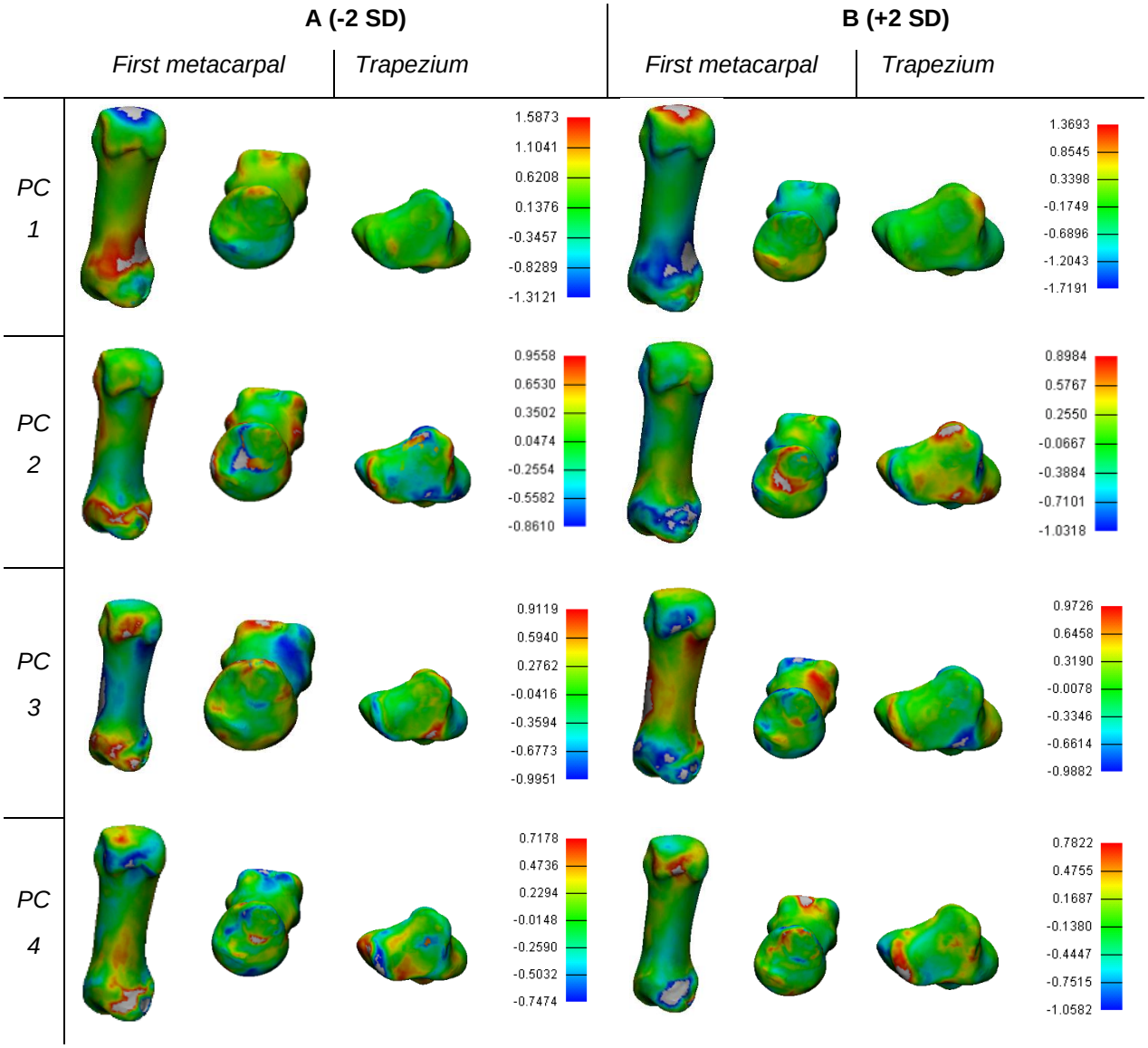

Figure 31 – Distances, in millimetres, between models for the first metacarpal and trapezium of the progressive T1 group, represented by seven PCs. The columns A exhibit the comparison between -2 SD and the mean model, while the columns B exhibit the comparison between +2 SD and the mean model. The colour grid represents the magnitude of the distances.

C

Table 11 – Morphologic parameters measured for the healthy population. For the first metacarpal, tilt and torsion angles were measured in degrees.

HEALTHY								
Weighing factor	**T0**				T1			
	PC 1		PC 2		PC 1		PC 2	
	Tilt	Torsion	Tilt	Torsion	Tilt	Torsion	Tilt	Torsion
+2 SD	1.90	8.40	2.86	-23.93	4.48	6.37	5.41	13.1
+1 SD	2.13	9.31	1.97	16.32	2.55	3.19	3.66	9.31
mean	0.36	10.49	0.36	10.49	0.55	14.96	0.55	14.96
-1 SD	-1.75	12.70	-0.27	15.30	-2.1	22.96	0.58	8.86
-2SD	-3.17	-5.68	-1.14	7.10	-3.51	18.14	-0.76	6.47

Table 12 – Morphologic parameters measured for the stabilised population. For the first metacarpal, tilt and torsion angles were measured in degrees.

STABILISED								
Weighing factor	**T0**				T1			
	PC 1		PC 2		PC 1		PC 2	
	Tilt	Torsion	Tilt	Torsion	Tilt	Torsion	Tilt	Torsion
+2 SD	7.26	7.26	-1.01	3.25	5.14	-2.67	3.12	6.07
+1 SD	6.74	12.31	-0.10	3.75	4.86	12.7	3.22	9.6
mean	4.53	12.48	4.53	12.48	2.28	9.89	2.28	9.89
-1 SD	3.32	16.60	10.44	15.90	3.14	19.43	3.95	15.25
-2SD	0.04	18.17	15.15	22.13	2.27	8.27	3.56	19.12

Table 13 – Morphologic parameters measured for the progressive population. For the first metacarpal, tilt and torsion angles were measured in degrees.

PROGRESSIVE								
Weighing factor	**T0**				T1			
	PC 1		PC 2		PC 1		PC 2	
	Tilt	Torsion	Tilt	Torsion	Tilt	Torsion	Tilt	Torsion
+2 SD	12.16	12.49	5.71	9.37	-3.22	-3.59	2.52	9.14
+1 SD	8.95	15.91	7.06	6.32	1.02	8.11	5.11	13.8
mean	5.37	15.02	5.37	15.02	5.89	12.99	5.89	12.99
-1 SD	-3.84	12.92	3.31	15.48	6.76	18.38	4.05	5.31
-2SD	-1.90	6.30	1.83	17.71	9.64	18.59	3.64	7.12

Table 14 – Morphologic parameters measured for the healhty population. For the trapezium, width and length were measured in milimetres.

HEALTHY								
Weighing factor	**T0**				T1			
	PC 1		PC 2		PC 1		PC 2	
	Length	Width	Length	Width	Length	Width	Length	Width
+2 SD	10,69	13,65	9,88	13,59	10,9	15,23	9,80	15,42
+1 SD	10,19	13,36	9,58	13,56	11,09	14,25	10,16	13,93
mean	11,26	14,01	11,26	14,01	10,58	14,59	10,58	14,59
-1 SD	11,04	14,24	10,81	13,28	10,35	14,17	11,06	13,96
-2SD	10,76	14,40	10,62	13,35	10,50	14,29	11,14	15,00

Table 15 – Morphologic parameters measured for the healhty population. For the trapezium, width and length were measured in milimetres.

STABILISED								
Weighing factor	**T0**				T1			
	PC 1		PC 2		PC 1		PC 2	
	Length	Width	Length	Width	Length	Width	Length	Width
+2 SD	9,01	13,43	10,13	13,61	9,92	12,68	9,14	14,32
+1 SD	10,51	12,88	10,16	13,25	12,04	13,19	9,61	13,25
mean	10,42	13,28	10,42	13,28	10,25	13,15	10,25	13,15
-1 SD	10,87	13,46	10,56	13,43	10,28	13,1	10,06	13,45
-2SD	11,02	14,22	11,6	13,65	10,26	13,48	10,81	13,56

Table 16 – Morphologic parameters measured for the healhty population. For the trapezium, width and length were measured in milimetres.

PROGRESSIVE								
Weighing factor	**T0**				T1			
	PC 1		PC 2		PC 1		PC 2	
	Tilt	Torsion	Tilt	Torsion	Tilt	Torsion	Tilt	Torsion
+2 SD	12,90	18,81	10,2	18,34	13,54	16,94	15	19,56
+1 SD	13,30	17,90	12,91	18,06	13,74	17,44	14,31	18,80
mean	13,86	17,16	13,86	17,16	13,87	19,08	13,87	19,08
-1 SD	13,64	17,36	13,69	17,17	10,44	13,87	13,46	17,21
-2SD	13,90	16,66	13,47	16,98	12,68	18,93	12,89	15,27